TUMOR BOUNDARY INSTABILITY INDUCED BY NUTRIENT CONSUMPTION AND SUPPLY

YU FENG, MIN TANG, XIAOQIAN XU, AND ZHENNAN ZHOU

ABSTRACT. We investigate the tumor boundary instability induced by nutrient consumption and supply based on a Hele-Shaw model derived from taking the incompressible limit of a cell density model. We analyze the boundary stability/instability in two scenarios: 1) the front of the traveling wave; 2) the radially symmetric boundary. In each scenario, we investigate the boundary behaviors under two different nutrient supply regimes, *in vitro* and *in vivo*. Our main conclusion is that for either scenario, the *in vitro* regime always stabilizes the tumor's boundary regardless of the nutrient consumption rate. However, boundary instability may occur when the tumor cells aggressively consume nutrients, and the nutrient supply is governed by the *in vivo* regime.

1. Introduction

Tumor, one of the major diseases threatening human life and health, has been widely concerned. The mathematical study of tumors has a long history and constantly active. We refer the reader to the textbook [10, 11] and review articles [2, 7, 48, 62]. Previous studies and experiments indicate that the shape of tumors is one of the critical criteria to distinguish malignant from benign. Specifically, malignant tumors are more likely to form dendritic structures than benign ones. Therefore, it is significant to detect and predict the formation of tumor boundary instability through mathematical models. Before discussing the mathematical studies of tumor morphology, we review relevant mathematical models as follows.

The first class of model was initiated by Greenspan in 1976 [32], which further inspired a mass of mathematical studies on tumor growth (e.g., [5, 8, 23, 65]). The tumor is regarded as an incompressible fluid satisfying mass conversation. More precisely, these free boundary type models have two main ingredients. One is the nutrient concentration σ governed by a reaction-diffusion equation, which considers the consumption by the cells and the supplement by vessels. The other main component is the internal pressure p, which further induces the cell velocity v via different physical laws (e.g., Darcy's law [5, 12, 26, 32], Stokes law [23, 28, 29], and Darcy&Stokes law [18, 19, 44, 60, 65]). Finally, the two ingredients are coupled via the mass conservation of incompressible tumor cells, which yields the relation $\nabla \cdot v = \lambda(\sigma)$, with the cell proliferation rate λ depending on σ. To close the model, the Laplace-Young condition ($p|_{\partial\Omega} = \gamma\kappa$, where κ is the mean curvature, and γ stands for the surface tension coefficient) is imposed on the tumor-host interface. For some variant models, people replace the Laplace-Young condition with other curvature-dependent boundary conditions (see, e.g., [50, 61, 64]). More sophisticated

---

models were also investigated recently. In particular, we mention the studies based on the two-phase models [50, 61, 64], and the works involve chemotaxis [34, 38].

Most studies on the stability/instability of tumor boundary are based on the above class of models and have been investigated from different points of view. Among them, for different models (e.g., Darcy [17, 21, 22, 25, 27]; and Stokes [20, 23, 24]), Friedman et al. proved the existence of non-radially symmetric steady states analytically and classified the stability/instability of the boundaries from the Hopf bifurcation point of view. Specifically, in their studies, the bifurcation parameter is characterized by the cell proliferation rate or ratio to cell-cell adhesiveness. Then the authors showed that the boundary stability/instability changes when the parameter crosses a specific bifurcation point. On the other hand, Cristini et al. in [12], as the pioneers, employ asymptotic analysis to study and predict the tumor evolution. Their work is of great significance to the dynamic simulation of tumors and nurtured more related works in this direction [49, 51, 52, 61, 64]. All the research demonstrated that many factors could induce the tumor's boundary instability, including but not limited to vascularization [12, 49, 50, 61], proliferation [12, 20, 24, 25, 27, 49], apoptosis [12, 20, 24, 25, 27, 49, 49, 61, 64], cell-cell adhesion [12, 20, 24, 25, 27, 61], bending rigidity [50, 64], microenvironment [51, 52, 61, 64], chemotaxis [49, 51].

In recent decades, tumor modeling from different perspectives has emerged and developed. In particular, one could consider the density model proposed by Byrne and Drasdo in [6], in which the tumor cell density ρ is governed by a porous medium type equation, and the internal pressure p is induced by the power rule $p = \rho^m$ with the parameter $m > 1$. The power rule enables p naturally vanish on the tumor boundary. Moreover, the boundary velocity v is governed by Darcy's law $v = -\nabla p|_{\partial\Omega}$. Previous research indicates that the porous media type equations have an asymptote concerning the parameter m tending to infinity [3, 30, 35, 41, 42]. Motivated by this, Perthame et al. derived the second kind of free boundary model in [57] by taking the incompressible limit (sending m to infinity), or equivalently mesa-limit of the density models. An asymptotic preserving numerical scheme was designed by J.Liu et al. in [45], the scheme naturally connects the numerical solutions to the density models to that of the free boundary models.

In the mesa-limit free boundary models proposed in [57], the limit density ρ_∞ can only take value in $[0, 1]$, and the corresponding limit pressure p_∞ is characterized by a monotone Hele-Shaw graph. More specifically, p_∞ vanishes on the unsaturated region where $\rho_\infty < 1$ (see equation (2.7)). The Hele-Shaw graph representation of pressure brings the following advantages. Firstly, in the Hele-Shaw type model, the formation of a necrotic core can be described by an obstacle problem [33], which leads ρ_∞ to decay exponentially in the necrotic core. Due to the Hele-Shaw graph, the pressure p_∞ naturally vanishes there instead of taking negative values. Secondly, a transparent regime called "patch solutions" exists, in which ρ_∞ remains in the form of $\chi_{D(t)}$, i.e., the indicator function of the tumor region. Again, to satisfy the corresponding Hele-Shaw graph, p_∞ has to vanish on the tumor's interface (where ρ_∞ drops from 1 to 0), which is significantly different from the first kind of free boundary models developed from [32], in which the internal pressure relies on the boundary curvature κ as mentioned previously. Moreover, in the mesa-limit free boundary models, the boundary velocity is still induced by Darcy's law $v_\infty = -\nabla p_\infty|_{\partial\Omega}$. For completeness, the derivation of the mesa-limit model is summarized in Section 2.1. Albeit various successful explorations based on such

mesa-limit free boundary models [13–16, 33, 36, 38–41, 43, 47, 54, 58, 59], the study on its boundary stability/instability is yet thoroughly open.

The primary purpose of this paper is to investigate whether boundary instability will arise in the mesa-limit free boundary models, which should shed light on the boundary stability of the cell density models when m is sufficiently large. To simplify the discussion, we consider tumors in the avascular stage with saturated cell density so that the density function ρ_∞ is a patch solution, and the tumor has a sharp interface. As the first attempt in this regard, we explore the instability caused by nutrient consumption and supply. A similar mechanism can induce boundary instability in other biological systems, see [4] for nutrient induce boundary instability in bacterial colony growth models. The role of nutrition in tumor models has been widely studied, and we refer the reader to the latest article in this direction [36]. Inspired by [58], we divide the nutrient models into two kinds, *in vitro* and *in vivo*, according to the nutrient supply regime. In either regime, the nutrient is consumed linearly in the tumor region with a rate $\lambda > 0$. However, in the *in vitro* model, we assume that a liquid surrounds the tumor with nutrient concentration c_B. Mathematically, the nutrient concentration remains c_B at the tumor-host interface. For the *in vivo* model, the nutrient is transported by vessels outside the tumor and reaches c_B at the far field. Correspondingly, we assume the exchange rate outside the tumor is determined by the concentration difference from the background, i.e., $c_B - c$. The two nutrient models will be specified more clearly in Section 2.1.2.

Our study of boundary stability/instability consists of two scenarios. We begin with a relatively simple case, the front of traveling waves, in which quantitative properties can be studied more explicitly. In this case, the unperturbed tumor region corresponds to a half plane with the boundary being a vertical line propagating with a constant normal velocity. Then we test the boundary stability/instability by adding a perturbation with frequency $l \in \mathbb{R}^+$ and amplitude δ. Our analysis shows that in the *in vitro* regime, δ always decreases to zero as time propagates. In other words, the boundary is stable for any frequency perturbation. In contrast, *in vivo* regime, there exists a threshold value L such that the perturbation with a frequency smaller than L becomes unstable when the nutrient consumption rate, λ, is larger than one.

The above case corresponds to the boundary stability/instability while the tumor is infinitely large. In order to further explore the influence of the finite size effect on the boundary stability/instability, we consider the perturbation of radially symmetric boundary with different wave numbers $l \in \mathbb{N}$ and radius R. Our analysis shows that the *in vitro* regime still suppresses the increase of perturbation amplitude and stabilizes the boundary regardless of the consumption rate, perturbation wave number, and tumor size. For the *in vivo* regime, when the consumption rate λ is less than or equal to one, the boundary behaves identically the same as the *in vitro* case. However, when λ is greater than one, the continuous growth of tumor radius will enable perturbation wave number to become unstable in turn (from low to high). Further more, as R is approaching infinity, the results in the radial case connect to the counterparts in the traveling wave case.

The main contribution of this work is to show that tumor boundary instability can be induced by nutrient consumption and supply. As a by-product, our results indicate that the cell apoptosis and curvature-dependent boundary conditions present

abundantly in previous studies (e.g., [12, 23]) are unnecessary for tumor boundary instability formation.

The paper is organized as follows. In Section 2, we first derive our free boundary models by taking the incompressible limit of density models characterized by porous medium type equations in Section 2.1. Besides that, we also introduce the *in vitro* and *in vivo* nutrient regimes in this subsection. Furthermore, the corresponding analytic solutions are derived in Section 2.2. Section 3 is devoted to introducing the linear perturbation technique in a general framework. Then, by using the technique in Section 3, we study the boundary stability of the traveling wave and the radially symmetric boundary under the two nutrient regimes, respectively, in Section 4 and Section 5 (with main results in Section 4.1 and Section 5.1). Finally, we summarize our results and discuss future research plans in Section 6.

2. **Preliminary**

2.1. **model introduction.**

2.1.1. *The cell density model and its Hele-Shaw limit.* To study the tumor growth under nutrient supply, let $\rho(x, t)$ denote the cell population density and $c(x, t)$ be the nutrient concentration. We assume the production rate of tumor cells is given by the growth function $G(c)$, which only depends on the nutrient concentration. On the other hand, we introduce

$$D(t) = \{\rho(x, t) > 0\} \tag{2.1}$$

to denote the support of ρ. Physically, it presents the tumoral region at time t. We assume the tumoral region expands with a finite speed governed by the Darcy law $v = -\nabla p$ via the pressure $p(\rho) = \rho^m$. Thus, the cell density ρ satisfies the equation:

$$\frac{\partial}{\partial t} \rho - \nabla \cdot (\rho \nabla p(\rho)) = \rho G(c), \quad x \in \mathbb{R}^2, \quad t \geqslant 0. \tag{2.2}$$

For the growth function $G(c)$, we assume

$$G(c) = G_0 c, \quad \text{with} \quad G_0 > 0, \tag{2.3}$$

note that in contrast to the nutrient models in [57, 63], we eliminate the possibility of the formation of a necrotic core by assuming that $G(\cdot)$ is always positive and linear (for simplicity), since this project aims to study the boundary instability induced by the nutrient distribution itself.

Many researches, e.g. [14, 15, 33, 39, 43, 57], indicate that there is a limit as $m \to \infty$ which turns out to be a solution to a free boundary problem of Hele-Shaw type. To see what happens, we multiply equation (2.2) by $m\rho^{m-1}$ on both sides to get

$$\frac{\partial}{\partial t} p(\rho) = |\nabla p(\rho)|^2 + mp(\rho)\Delta p(\rho) + mG_0 p(\rho)c. \tag{2.4}$$

Hence, if we send $m \to \infty$, we formally obtain the so called *complementarity condition* (see [14, 57] for a slight different model):

$$p_\infty(\Delta p_\infty + G_0 c) = 0. \tag{2.5}$$

On the other hand, the cell density $\rho(x, t)$ converges to the weak solution (see [57]) of

$$\frac{\partial}{\partial t} \rho_\infty - \nabla \cdot (\rho_\infty \nabla p_\infty) = \rho_\infty G(c), \tag{2.6}$$

and p_∞ compels the limit density ρ_∞ only take value in the range of $[0,1]$ for any initial date $\rho_0 \in [0,1]$ (see Theorem 4.1 in [57] for a slightly different model). Moreover, the limit pressure p_∞ belongs to the Hele-Shaw monotone graph:

$$(2.7) \qquad p_\infty(\rho_\infty) = \left\{ \begin{array}{ll} 0, & 0 \leqslant \rho_\infty < 1, \\ [0,\infty), & \rho_\infty = 1. \end{array} \right.$$

The incompressible limit and the *complementarity condition* of a fluid mechanical related model have been rigorously justified in [14, 57]. And the incompressible limit of (2.2) (coupled with nutrient models that will be introduced in the next section) was verified numerically in [46].

We define the support of p_∞ to be

$$(2.8) \qquad D_\infty(t) = \{p_\infty(x,t) > 0\},$$

then (2.5) and (2.7) together yield

$$(2.9a) \qquad -\Delta p_\infty = G_0 c \qquad \text{for} \quad x \in D_\infty(t),$$

$$(2.9b) \qquad p_\infty = 0, \qquad \text{for} \quad x \in \mathbb{R}^2 \setminus D_\infty(t),$$

and $\rho_\infty = 1$ in D_∞. Therefore, once the nutrient concentration $c(x,t)$ is known one can recover p_∞ from the elliptic equation above.

Now we justify the relationship between $D(t)$ and $D_\infty(t)$. Observe that when m is finite, ρ and $p(\rho)$ have the same support $D(t)$, whereas as m tends to infinity, ρ_∞ may have larger support than p_∞. However, a large class of initial data, see e.g. [56], enable the free boundary problem (correspond to (2.6) and (2.9)) possess patch solutions, i.e., $\rho_\infty = \chi_{D_\infty}$, where χ_A stands for the indicator function of the set A. In this case, the support of p_∞ coincides with that of ρ_∞. Moreover, the boundary velocity v is governed by Darcy law $v = -\nabla p_\infty$. Further, the boundary moving speed along the normal direction at the boundary point x, denote by $\sigma(x)$, is given by:

$$(2.10) \qquad \sigma(x) = -\nabla p_\infty \cdot \hat{n}(x),$$

where $\hat{n}(x)$ is the outer unit normal vector at $x \in \partial D_\infty(t)$. The boundary speed for more general initial data was studied in [39].

As the end of this subsection, we emphasize that in our free boundary model, as the limit of the density models, the pressure p_∞ always vanishes on ∂D_∞. However, as mentioned previously, in the first kind free boundary models, the internal pressure $\tilde{p}$ is assumed to satisfy the so-called Laplace-Young condition (or some other curvature dependent boundary condition). Mathematically, the boundary condition (2.9b) is replaced by

$$(2.11) \qquad \tilde{p}(x) = \gamma \kappa(x),$$

where $\gamma > 0$ is a constant coefficient, and $\kappa(x)$ denotes the curvature at the boundary point x. In the related studies, the curvature condition (2.11) plays an essential role (e.g., [12, 23]).

2.1.2. *Two nutrient models.* Regarding the nutrient, it diffuses freely over the two dimensional plane. However, inside the tumoral region, the cells consume the nutrient. While outside the tumor, the nutrient exchanges with the far field concentration c_B provided by the surrounding environment or vasculature. It follows

that the following reaction-diffusion equation can govern the consumption, exchange, and diffusion of the nutrient in general:

$$\tau \partial_t c - \Delta c + \Psi(\rho, c) = 0, \tag{2.12}$$

where τ is the characteristic time scale of the nutrient change, and $\Psi(\rho, c)$ describes the overall effects of the nutrient supply regime outside the tumor and the nutrient consumption by cells inside the tumor. To simplify the mathematical analysis, we drop the time derivative in (2.12) and consider following elliptic formulation instead

$$-\Delta c + \Psi(\rho, c) = 0. \tag{2.13}$$

This is reasonable because $\tau \ll 1$ (see, e.g., [1, 5, 31]). As in [58], two specific developed and widely studied models are the *in vitro* and the *in vivo* model.

For the *in vitro* model, we assume that the tumor is surrounded by a liquid in which the exchange rate with the background is so fast that the nutrient concentration can be assumed to be the same constant c_B as that of the surrounding liquid, while inside the tumoral region, the consumption function is bi-linear in both the concentration c and the cell density ρ with consumption rate $\lambda > 0$. The boundary instability was observed in models where tissues aggressively consume nutrients [53]. Therefore, in our models, we expect boundaries are more likely to be unstable when λ is large. When the *in vitro* is coupled with the cell density model (2.2), equation (2.13) writes

$$-\Delta c + \lambda \rho c = 0, \qquad \text{for} \quad x \in D(t), \tag{2.14a}$$

$$c = c_B, \qquad \text{for} \quad x \in \mathbb{R}^2 \setminus D(t). \tag{2.14b}$$

By considering the incompressible limit of the density model (sending $m \to \infty$), and concern patch solutions $\rho_\infty = \chi_{D_\infty}$. Equation (2.14) tends to:

$$-\Delta c + \lambda c = 0, \qquad \text{for} \quad x \in D_\infty(t), \tag{2.15a}$$

$$c = c_B, \qquad \text{for} \quad x \in \mathbb{R}^2 \setminus D_\infty(t). \tag{2.15b}$$

For the *in vivo* model, the consumption of nutrients within the tumor region (where $\rho > 0$) remains the same as in the *in vitro* model. However, in the *in vivo* model, the nutrients are provided by vessels of the healthy tissue surrounding the tumor, while the healthy tissue consumes nutrients as well. This leads to the nutrient supply outside the tumor being determined by the concentration difference from the background, $c_B - c$, with a positive coefficient $\tilde{\lambda}$. Mathematically, the overall function $\Psi(\rho, c)$ is written as $\Psi(\rho, c) = \lambda \rho c \cdot \chi_D - \tilde{\lambda}(c_B - c) \cdot \chi_{D^c}$. For simplicity, we set $\tilde{\lambda} = 1$ and $\lambda > 0$. Note that this expression guarantees the nutrient concentration reaches c_B at the far field. A more detailed discussion of this issue can be found in [9, 37].

With the same reason as the previous case, by taking $m \to \infty$ in the density model and concerning patch solutions, we get the *in vivo* nutrient equations for the limit free boundary model,

$$-\Delta c + \lambda c = 0, \qquad \text{for} \quad x \in D_\infty(t), \tag{2.16a}$$

$$-\Delta c = c_B - c, \qquad \text{for} \quad x \in \mathbb{R}^2 \setminus D_\infty(t). \tag{2.16b}$$

Moreover, we need to emphasize that the *in vivo* we refer to is different from the previous articles (see, e.g., [12]) in which *in vivo* corresponds to the vascularization inside the tumor.

The uneven growth phenomena in the tumor models are conjectured due to the non-uniform distribution of nutrients [53]. More precisely, in contrast to the fingertips region, the nutrient is inadequate around the valley since more cells consume nutrients there. Consequently, the tissue around the tips grows faster than the valleys, and therefore instability occurs. In the *in vitro* model, the concentration of the nutrient will match the background concentration c_B at the boundary regardless of the regions. However, for the *in vivo* model, the nutrient is directly available only from healthy tissue; this regime will enlarge the concentration difference at the tips and valleys. Therefore, we expect tumor borders are more prone to grow unevenly in the *in vivo* models, in particular when the consumption rate λ is relatively large.

2.2. **Analytic solutions.** Starting from this section, we focus on the mesa limit free boundary models. Therefore, for simplicity of the notations, we drop the free boundary models' subscripts and use $D(t)$, ρ, and p to denote the tumoral region, cell density, and pressure in the limit model. On the other hand, through this paper, we use I_j and K_j ($j \in \mathbb{N}$) to denote the second kind of modified Bessel functions, their definitions and basic properties are reviewed in Appendix A.

The models introduced in Section 2.1 have been studied in [46] when $\lambda = 1$. In particular, the authors derived $2D$ radially symmetric solutions for the free boundary models, which are coupled with either the *in vitro* or the *in vivo* model. Moreover, their computation yields that as the radius of the tumor tends to infinity, the boundary velocity tends to be a finite constant. In other words, the radially symmetric solutions converge to traveling wave solutions.

For self-consistency, we recall the derivation of the radially symmetric solutions in [46] in this section. Besides that we also derive the traveling wave solutions for the two nutrient models and verify that they are indeed the limit of the radially symmetric solutions as radius goes to infinity. The analytical solutions in this section will serve as the cornerstone of subsequent perturbation analysis. Now, we begin with the traveling wave scenario.

2.2.1. *traveling plane solution for the* in vitro *model.* For solving two-dimensional traveling wave solutions, we fix the traveling front at $\xi = x - \sigma t = 0$, where σ stands for the traveling speed and will be determined later. Without loss of generality, let the tumoral region be the left half plane, that is $D(t) = \{(\xi, y) | \xi \leqslant 0\}$. One can easily see that in the unperturbed two-dimensional problem, to find its solution reduces to solve a one-dimensional problem. Moreover, we disclose that the variable y will serve as the perturbation parameter in the perturbation problems, which will be investigated later. The one dimensional problem writes:

$$-\partial_\xi^2 c + \lambda c = 0, \quad \text{for} \quad \xi \leqslant 0, \tag{2.17a}$$

$$c = c_B, \quad \text{at} \quad \xi = 0, \tag{2.17b}$$

in addition, we also assume the concentration of nutrient vanish at the center of tumor, that is

$$c(\xi) = 0, \quad \text{for} \quad \xi = -\infty. \tag{2.17c}$$

And the equations for pressure $p(\xi, y)$, i.e., (2.9) and (2.10) reads

$$-\partial_\xi^2 p = G_0 c, \quad \text{for} \quad \xi \leqslant 0, \tag{2.18a}$$

$$p = 0, \quad \text{for} \quad \xi \geqslant 0, \tag{2.18b}$$

and traveling speed is given by

$$\sigma = -\partial_\xi p(0). \tag{2.18c}$$

Since the gradient of the pressure is always equal to zero at the center of the tumor, we also have

$$\partial_\xi p(\xi) = 0, \qquad \text{for} \quad \xi = -\infty. \tag{2.18d}$$

By solving (2.17) we get

$$c = c_B e^{\sqrt{\lambda}\xi}, \qquad \text{for} \quad \xi \leqslant 0, \tag{2.19}$$

plug the above expression into (2.18) to solve for p and get:

$$p(\xi) = -\frac{G_0 c_B}{\lambda} e^{\sqrt{\lambda}\xi} + \frac{G_0 c_B}{\lambda} \qquad \text{for} \quad \xi \leqslant 0. \tag{2.20}$$

Then, we can further find the traveling speed

$$\sigma = -\partial_\xi p(0) = \frac{G_0 c_B}{\sqrt{\lambda}}. \tag{2.21}$$

2.2.2. *traveling plane solution for the* in vivo *model.* For the *in vivo* model, the only difference from the *in vitro* model is the equations for $c(\xi, y)$ are replaced by

$$-\partial_\xi^2 c + \lambda c = 0, \qquad \text{for} \quad \xi \leqslant 0, \tag{2.22a}$$

$$-\partial_\xi^2 c = c_B - c, \qquad \text{for} \quad \xi \geqslant 0, \tag{2.22b}$$

$$c(\xi) = 0, \qquad \text{for} \quad \xi = -\infty. \tag{2.22c}$$

in addition, c and $\partial_\xi c$ are both continuous at the boundary of the tumor, that is

$$c(0^-) = c(0^+) \quad \text{and} \quad \partial_\xi c(0^-) = \partial_\xi c(0^+). \tag{2.22d}$$

And the pressure p still satisfies (2.18).

By solving (2.22) we get

$$c(\xi) = \begin{cases} \frac{c_B}{\sqrt{\lambda}+1} e^{\sqrt{\lambda}\xi} \overset{\text{def}}{=} c^{(\mathrm{i})}(\xi) & \text{for} \quad \xi \leqslant 0, \\ -\frac{\sqrt{\lambda}c_B}{\sqrt{\lambda}+1} e^{-\xi} + c_B \overset{\text{def}}{=} c^{(\mathrm{o})}(\xi) & \text{for} \quad \xi \geqslant 0. \end{cases} \tag{2.23}$$

and plug the above expression into (2.18) to derive p and get

$$p(\xi) = -\frac{G_0 c_B}{\lambda(\sqrt{\lambda}+1)} e^{\sqrt{\lambda}\xi} + \frac{G_0 c_B}{\lambda(\sqrt{\lambda}+1)} \qquad \text{for} \quad \xi \leqslant 0. \tag{2.24}$$

And the boundary speed is given by

$$\sigma = -\partial_\xi p(0) = \frac{G_0 c_B}{\lambda + \sqrt{\lambda}}. \tag{2.25}$$

By now, we have finished the derivation for the traveling wave solutions. In the next two subsections, we recall the derivation for the radially symmetric scenario in [46] and verify that the boundary speeds converge to the traveling waves' for the corresponding nutrient regime.

2.2.3. *2D radially symmetric model for the* in vitro *model.* For the radially symmetric free boundary model, the tumoral region becomes $D(t) = \mathbb{B}_{R(t)}(0)$ (a disk centered at origin with radius R). In this case, we employ polar coordinates (r, θ), and we can conclude that the solutions are independent of θ by symmetry. However the variable θ will play an important role in the perturbed problem, which will be seen in the later sections. Thus, for the free boundary model with nutrients governed by the *in vitro* model, equation (2.15) can be further written as

$$-\frac{1}{r}\partial_r(r\partial_r c) + \lambda c = 0, \qquad \text{for} \quad r \leqslant R(t), \tag{2.26a}$$

$$c = c_B, \qquad \text{for} \quad r \geqslant R(t). \tag{2.26b}$$

And the equations for pressure p (2.9) and (2.10) reads

$$-\frac{1}{r}\partial_r(r\partial_r p) = G_0 c \qquad \text{for} \quad r \leqslant R(t), \tag{2.27a}$$

$$p = 0, \qquad \text{for} \quad r \geqslant R(t), \tag{2.27b}$$

$$\sigma(R(t)) = -\partial_r p(R(t)), \qquad \text{on} \quad \partial \mathbb{B}_R(0). \tag{2.27c}$$

And by symmetry, we also require

$$\partial_r p(0) = 0. \tag{2.27d}$$

By solving (2.26) we get

$$c(r, t) = c_B \frac{I_0(\sqrt{\lambda} r)}{I_0(\sqrt{\lambda} R)} \qquad \text{for} \quad r \leqslant R(t). \tag{2.28}$$

Plug the above expression into (2.27) to solve for p, and we get:

$$p(r, t) = -\frac{G_0 c_B}{\lambda I_0(\sqrt{\lambda} R(t))} I_0(\sqrt{\lambda} r) + \frac{G_0}{\lambda} c_B \qquad \text{for} \quad r \leqslant R(t). \tag{2.29}$$

And the boundary velocity is given by

$$\dot{R} = \sigma(R(t)) = -\frac{\partial p}{\partial r}(R(t)) = \frac{G_0 c_B I_1(\sqrt{\lambda} R)}{\sqrt{\lambda} I_0(\sqrt{\lambda} R)}. \tag{2.30}$$

Note that as $R(t) \to \infty$ the speed limit is $\frac{G_0 c_B}{\sqrt{\lambda}}$, which recovers the speed for the traveling wave solution (2.21).

2.2.4. *2D radially symmetric model for the* in vivo *model.* The computation is similar to the previous case, except that the equations for nutrient are replaced by

$$-\frac{1}{r}\partial_r(r\partial_r c) + \lambda c = 0, \qquad \text{for} \quad r \leqslant R(t), \tag{2.31a}$$

$$-\frac{1}{r}\partial_r(r\partial_r c) = c_B - c, \qquad \text{for} \quad r \geqslant R(t). \tag{2.31b}$$

By solving above two equations and using the continuity of both c and $\partial_r c$ at $R(t)$, we get

$$c(r, t) = \begin{cases} c_B a_0(R) I_0(\sqrt{\lambda} r) \overset{\text{def}}{=} c^{(i)}(r, t), & \text{for} \quad r \leqslant R(t), \\ c_B(1 + b_0(R) K_0(r)) \overset{\text{def}}{=} c^{(o)}(r, t), & \text{for} \quad r \geqslant R(t), \end{cases} \tag{2.32}$$

where a_0 and b_0 are given by

$$a_0(R) = \frac{K_1(R)}{\sqrt{\lambda} K_0(R) I_1(\sqrt{\lambda} R) + K_1(R) I_0(\sqrt{\lambda} R)} \overset{\text{def}}{=} \frac{K_1(R)}{C(R)}, \tag{2.33a}$$

$$(2.33b) \qquad b_0(R) = -\frac{\sqrt{\lambda}I_1(R)}{\sqrt{\lambda}K_0(R)I_1(\sqrt{\lambda}R) + K_1(R)I_0(\sqrt{\lambda}R)} \stackrel{\text{def}}{=\!=} -\frac{\sqrt{\lambda}I_1(R)}{C(R)}.$$

Then from the pressure equations (2.27), we can solve and get

$$(2.34) \quad p(r,t) = -\frac{G_0 c_B}{\lambda}a_0(R)I_0(\sqrt{\lambda}r) + \frac{G_0 c_B}{\lambda}a_0(R)I_0(\sqrt{\lambda}R), \qquad \text{for} \quad r \leqslant R(t).$$

And the velocity of the boundary is given by

$$(2.35) \quad \dot{R} = \sigma(R(t)) = \frac{G_0 c_B K_1(R)I_1(\sqrt{\lambda}R)}{\lambda K_0(R)I_1(\sqrt{\lambda}R) + \sqrt{\lambda}K_1(R)I_0(\sqrt{\lambda}R)} \leqslant \frac{G_0 c_B I_1(\sqrt{\lambda}R)}{\sqrt{\lambda}I_0(\sqrt{\lambda}R)},$$

which implies that the speed in the *in vivo* model is slower than that in the *in vitro* model. Again, by sending $R \to \infty$, we get the limiting speed for the *in vivo* model is $\frac{c_B G_0}{\lambda + \sqrt{\lambda}}$, which recovers the speed for the traveling wave in (2.25).

3. **Framework of the perturbation analysis**

We devote this section to establishing the general framework of our asymptotic analysis. Such analysis involves classical techniques which was originally developed by Mullins et al. in [55] and widely used in [12, 49, 51, 52, 61, 64], whereas we present it as generic methodology which in theory can be applied to other problems as well.

We divide our analysis into three parts as follows.

3.1. **Perturbation of the boundary.** We study the perturbation of two kinds of boundaries, the radial boundary and the front of traveling waves, and the relationship between them. In either case, we have a proper coordinate system denoted as (ζ, ϑ). For simplicity, we assume the boundary profile is a curve $\mathcal{O}_t \subseteq \mathbb{R}^2$, which can be parameterized by the variable ϑ in the following form:

$$(3.1) \qquad \mathcal{O}_t(\vartheta) = \{(\zeta, \vartheta)|\zeta = \mathcal{Z}(t,\vartheta), \vartheta \in \mathcal{R}\}$$

with some contour index function $\mathcal{Z}(t,\vartheta)$ and range $\mathcal{R}$.

For the radial case, the unperturbed tumor region at time t is given by a disk with radius $R(t)$, that is $D(t) = \mathbb{B}_{R(t)}$. In this case, equations and functions are naturally presented in terms of the polar coordinate. Therefore, $(\zeta, \vartheta) = (r, \theta)$ and $\mathcal{R} = [-\pi, \pi)$. Further more, the tumor boundary at time t can be written as:

$$(3.2) \qquad \mathcal{B}_t(\theta) = \{(r, \theta)|r = R(t), \theta \in [-\pi, \pi)\}.$$

For the traveling wave case, we employ the Euler coordinate (ξ, y) (where $\xi = x - \sigma t$). In this case, the tumor region is a half plane with a moving front. We fix the front (propagate to the right) at $\xi = 0$ with traveling speed σ, and the tumor region, therefore, become $D(t) = \{(\xi, y)|\xi \leqslant 0\}$. Then, we write the traveling front more clearly in the parameter curve form:

$$(3.3) \qquad \mathcal{B}(y) = \{(\xi, y)|\xi = 0, y \in \mathbb{R}\}.$$

For the purpose of introducing perturbation method in a general framework, we combine the two scenarios above in the following unified notations. Let $D(t)$ still presents the tumor region at time t; and the boundary curve writes

$$(3.4) \qquad \mathcal{B}_t(\vartheta) = \{(\zeta, \vartheta)|\zeta = Z(t), \vartheta \in \mathcal{R}\}.$$

Moreover, any point $B \in \mathcal{B}_t$ can be presented as $B(Z, \vartheta_*)$ for some $\vartheta_* \in \mathcal{R}$. Note that in either case above, the index function $Z(t)$ is independent on the parameter

variable ϑ. More precisely, for the radial case $Z(t) = R(t)$, and (3.4) stands for (3.2); for the traveling wave case, (3.4) stands for (3.3) with $Z(t)$ takes constant value 0.

Next, we add a small perturbation to the two kinds of boundaries. From the parameterization representation point of view, the perturbation replaces the boundary curve (3.4) by:

$$\tag{3.5} \tilde{\mathcal{B}}_t(\vartheta) = \{(\zeta, \vartheta) | \zeta = Z(t) + \delta(t)\mathcal{P}(\vartheta), \vartheta \in \mathcal{R}\},$$

where $\delta(t) \ll 1$ stands for the amplitude of the perturbation, and $\mathcal{P}(\vartheta)$ characterizes the perturbation profile. Thus, the perturbed boundary at time t is still parameterized by the variable ϑ. Intuitively, (3.5) means that the perturbation will push the point $(Z, \vartheta_*) \in \mathcal{B}_t$ to $(Z + \delta\mathcal{P}(\vartheta_*), \vartheta_*) \in \tilde{\mathcal{B}}_t$ for any $\vartheta_* \in \mathcal{R}$. Note that the perturbation form (3.5) enables the evolution of the perturbation term to reduce to the evolution of the amplitude function $\delta(t)$ while its spatial profile persists. Such an ansatz with temporal and spatial degrees of freedom separated makes sense only when the profile function represents a typical model of a general classical of contours. In the next, we explain how to choose the perturbation profiles in the two cases.

In the radial symmetry case, the profile $\mathcal{P}(\theta)$ is parameterized by $\theta \in [-\pi, \pi)$ and it can be expressed as a Fourier expansions in general. In particular, for the single wave perturbation with wave number l, $\mathcal{P}(\theta)$ takes the form of:

$$\tag{3.6} \mathcal{P}(\theta) = C_1 \cos l\theta + C_2 \sin l\theta, \quad \text{with} \quad l \in \mathbb{N}^+,$$

where C_1, C_2 are constant coefficients. Note that by rotating the coordinate system and rescaling on $\delta(t)$, without loss of generality we can simply take

$$\tag{3.7} \mathcal{P}(\theta) = \cos l\theta \stackrel{\text{def}}{=} \mathcal{P}_l(\theta).$$

For the traveling wave case, the profile is parameterized by $y \in \mathbb{R}$. By a similar reason to the radial case, we can simply consider

$$\tag{3.8} \mathcal{P}_l(y) = \cos ly, \quad \text{with} \quad l \in \mathbb{R}^+,$$

otherwise we can just shift the profile along y-axis.

It is important to note that for the perturbation of the traveling wave, we are actually allowed to take $\mathcal{P}(y) = \cos ly$ with $l \in \mathbb{R}^+$. However, only integer frequencies perturbation are reasonable for the radial case, since $\mathcal{P}(\theta)$ has to be a 2π-periodic function.

3.2. **Solutions after perturbation.** Let $\tilde{D}(t)$, enclosed by $\tilde{\mathcal{B}}_t$, denote the tumoral region after the perturbation. Then the perturbed functions $(\tilde{c}, \tilde{p}, \tilde{\rho})$ satisfy the equations (boundary conditions will be specified in the next subsection):

$$\tag{3.9a} -\Delta\tilde{c} + \Psi(\tilde{\rho}, \tilde{c}) = 0, \qquad \text{on} \quad \mathbb{R}^2,$$

$$\tag{3.9b} -\Delta\tilde{p} = G_0\tilde{c}, \qquad \text{in} \quad \tilde{D}(t),$$

recall that $\Psi(\tilde{\rho}, \tilde{c})$ reads (2.15) in the *in vitro* model and (2.16) in the *in vivo* model. When the boundary perturbation vanishes, (3.9) reduce to the the unperturbed problem, where the solutions are given in a closed-form. In the presence of the boundary perturbation, we still have $\tilde{\rho} = \chi_{\tilde{D}}$ since it remains as a patch, but the solution to $\tilde{c}$ and $\tilde{p}$ are no longer available. However, we can alternatively seek asymptotic solutions of $\tilde{c}$ and $\tilde{p}$ with respect to δ, while the condition $\tilde{\rho} = \chi_{\tilde{D}}$ help to linearize the calculation. We elaborate the asymptotic analysis procedures as follows.

Firstly, corresponding to the small perturbation (3.5), we have the following asymtotic expansion with respect to the small value δ:

$$(3.10a) \qquad \tilde{c}(\zeta, \vartheta, t) = c_0(\zeta, t) + \delta c_1(\zeta, \vartheta, t) + O(\delta^2),$$

$$(3.10b) \qquad \tilde{p}(\zeta, \vartheta, t) = p_0(\zeta, t) + \delta p_1(\zeta, \vartheta, t) + O(\delta^2).$$

Since the perturbation scale is assumed to be very small, i.e., $\delta \ll 1$, the behavior of the perturbed solutions are dominated by the unperturbed ones. Thus, the leading order terms $c_0(\zeta, t)$ and $p_0(\zeta, t)$ take the same expression as the solutions without perturbation, which have been solved in Section 2.2. On the other hand, the main response corresponding to the perturbation are captured by the first-order terms $c_1(\zeta, \vartheta, t)$ and $p_1(\zeta, \vartheta, t)$. Note that besides variable ζ they depend on ϑ as well.

We continue to investigate the structures of c_1 and p_1 when the perturbation profile (3.5) is given by $\mathcal{P}(\vartheta) = \mathcal{P}_l(\vartheta)$, here $\mathcal{P}_l(\vartheta)$ presents (3.7) or (3.8) in the respective case. In either case, the perturbed tumoral region $\tilde{D}$ still possess a symmetry, or periodicity, respect to the parameter ϑ (θ for the radial case and y for the traveling wave case). Then we have following conclusion for the perturbed solutions $(\tilde{c}, \tilde{p})$.

Lemma 3.1. *If the perturbed solutions are unique, then they must process the same periodicity as the boundary geometry.*

Proof. For either scenario, the front of traveling wave or radially symmetric boundary, we assume the boundary has periodicity ϑ^*. Then, with respect to (3.5) we have:

$$(3.11) \qquad \zeta(\vartheta) = \zeta(\vartheta + \vartheta^*),$$

where $\zeta(\vartheta) \overset{\text{def}}{=} Z(t) + \delta \mathcal{P}(\vartheta)$. For $\mathcal{P}(\vartheta) = \cos l\vartheta$, ϑ^* is given by $\vartheta^* = \frac{2\pi}{l}$. We define the translation operator $\tau_{\vartheta^*}(\zeta, \vartheta) : (\zeta, \vartheta) \mapsto (\zeta, \vartheta + \vartheta^*)$. One can easily observe that the nutrient equations (for either *in vitro* or *in vivo*) and the pressure equation are both invariant under τ_{ϑ^*} since the operator simply corresponds to a translation or a rotation, and diffusion operator is isotropic. Moreover, the boundary geometry and boundary conditions remain the same under the operator τ_{ϑ^*} as well. Thus, the uniqueness of the solution yield that the unique solutions c^* and p^* must possess the same periodicity as the boundary geometry. That is,

$$(3.12a) \qquad c^*(\zeta, \vartheta) = c^*(\tau_{\vartheta^*}(\zeta, \vartheta)),$$

$$(3.12b) \qquad p^*(\zeta, \vartheta) = p^*(\tau_{\vartheta^*}(\zeta, \vartheta)).$$

$\square$

According to the above lemma, to be consistent with the boundary's periodicity, we expand $c_1(\zeta, \vartheta, t)$ and $p_1(\zeta, \vartheta, t)$ as Fourier series, and (3.10) can be further written as:

$$(3.13a) \qquad \tilde{c}(\zeta, \vartheta, t) = c_0(\zeta, t) + \delta(t)\Sigma_{k=1}^{\infty} c_1^k(\zeta, t)\mathcal{P}_l^k(\vartheta) + O(\delta^2),$$

$$(3.13b) \qquad \tilde{p}(\zeta, \vartheta, t) = p_0(\zeta, t) + \delta(t)\Sigma_{k=1}^{\infty} p_1^k(\zeta, t)\mathcal{P}_l^k(\vartheta) + O(\delta^2),$$

where $\mathcal{P}_l^k(\vartheta) = \cos kl\vartheta$. In the above expansions, $c_1^k(\zeta, t)$ and $p_1^k(\zeta, t)$ (with $k \in \mathbb{N}^+$) serve as the Fourier coefficients with $O(1)$. From the calculation in the later sections (Section 4.2 and Section 5.2), we will see that only c_1^1 and p_1^1, the coefficients of the wave number that is the same as the perturbation, do not vanish. Therefore, it

suffices to keep the first term in the series (3.13) and drop the superscript in c_1^1, p_1^1 and, $\mathcal{P}_l^1$. Thus, (3.13) writes

$$\tilde{c}(\zeta, \vartheta, t) = c_0(\zeta, t) + \delta(t)c_1(\zeta, t)\mathcal{P}_l(\vartheta) + O(\delta^2), \tag{3.14a}$$

$$\tilde{p}(\zeta, \vartheta, t) = p_0(\zeta, t) + \delta(t)p_1(\zeta, t)\mathcal{P}_l(\vartheta) + O(\delta^2). \tag{3.14b}$$

In the traveling wave case, the dependency of t can be removed for the terms c_j and p_j $(j = \{0, 1\})$, since the unperturbed tumor boundary do not evolve in time. Finally, by plugging the expansion (3.14) into (3.9) and collect the first order terms we get

$$-\Delta(c_1(\zeta, t)\mathcal{P}_l(\vartheta)) + \lambda c_1(\zeta, t)\mathcal{P}_l(\vartheta) = 0, \quad \text{in} \quad \tilde{D}(t), \tag{3.15a}$$

$$-\Delta(p_1(\zeta, t)\mathcal{P}_l(\vartheta)) = G_0(c_1(\zeta, t)\mathcal{P}_l(\vartheta)), \quad \text{in} \quad \tilde{D}(t), \tag{3.15b}$$

for either nutrient regime. In addition, for the *in vivo* model c_1 also satisfies

$$-\Delta(c_1(\zeta, t)\mathcal{P}_l(\vartheta)) + c_1(\zeta, t)\mathcal{P}_l(\vartheta) = 0, \quad \text{in} \quad \mathbb{R}^2 \setminus \tilde{D}(t). \tag{3.15c}$$

where we used the fact that the zero order terms satisfy (3.9). By solving (3.15), one can get the solutions of c_1 and p_1 for the respective models. Note that (3.15) implies the expression of c_1 and p_1 depend on the wave number l. The detailed computation will be carried out for the specific cases in the later sections.

3.3. **Match the boundary condition.** In the last part of this section, we explain how to determine the particular solutions of c_1 and p_1 by matching the boundary conditions. We also show that by using the expression of p_1, one can determine the evolution of the perturbation magnitude.

In this section, we always assume the perturbation profile $\mathcal{P}(\vartheta)$ is given by $\mathcal{P}_l(\vartheta)$. And note that given t for any $\vartheta \in \mathcal{R}$, $(Z + \delta\mathcal{P}_l(\vartheta), \vartheta)$ presents a point on the perturbed boundary $\tilde{\mathcal{B}}_t$, which is originally at the position $(Z, \vartheta) \in \mathcal{B}_t$. Recall that c_0 and c_1 (similarly for p_0 and p_1) only depend on the variable ζ in space, and the unperturbed boundary $\mathcal{B}_t$ is characterized as the contour of ζ with level set index $Z(t)$ (see (3.4)).

Since the analytical solutions are not available for the perturbed problem, it is not practical to enforce the boundary conditions in the precise way. Instead, since we seek the first order perturbation solutions due to the boundary variation, we can approximately match the the perturbed solutions at the perturbed boundary up to $O(\delta^2)$ error with the their evaluations at the unperturbed boundary.

For the *in vitro* model, the perturbed solution $\tilde{c}$ satisfies the boundary condition:

$$\tilde{c} = c_B, \quad \text{at} \quad \tilde{\mathcal{B}}_t. \tag{3.16}$$

Thus by using expansion (3.14a), we can evaluate $\tilde{c}$ at the perturbed boundary point $(Z + \delta\mathcal{P}_l(\vartheta), \vartheta)$ to get

$$\begin{aligned} \tilde{c}(Z + \delta\mathcal{P}_l(\vartheta), \vartheta, t) &= c_0(Z + \delta\mathcal{P}_l(\vartheta), t) + \delta c_1(Z + \delta\mathcal{P}_l(\vartheta), t)\mathcal{P}_l(\vartheta) + O(\delta^2) \\ &= c_0(Z, t) + \delta\partial_\zeta c_0(Z, t)\mathcal{P}_l(\vartheta) + \delta c_1(Z, t)\mathcal{P}_l(\vartheta) + O(\delta^2), \end{aligned} \tag{3.17}$$

where we used the Taylor expansions for $c_0(Z + \delta\mathcal{P}_l, t)$ and $c_1(Z + \delta\mathcal{P}_l, t)$. By the boundary conditions of the perturbed and unperturbed problems, we have $\tilde{c}(Z + \delta\mathcal{P}_l(\vartheta), \vartheta, t) = c_0(Z, t) = c_B$ for arbitrary $\vartheta \in \mathcal{R}$. Thus the zero order terms in (3.17) are canceled out, and by balancing the first order terms in (3.17) we get

$$\partial_\zeta c_0(Z, t) + c_1(Z, t) = 0. \tag{3.18}$$

While for the *in vivo* model, $\tilde{c}$ and its normal derivative are both continuous at $\tilde{\mathcal{B}}_t$. And in either kind of boundary, the normal derivative of $\tilde{c}(\zeta, \vartheta, t)$ on $\tilde{\mathcal{B}}_t$ is given by $\partial_\zeta \tilde{c}(\zeta, \vartheta, t)$ for any $\tilde{B}(\zeta, \vartheta) \in \tilde{\mathcal{B}}_t$. And if we decompose the solution $\tilde{c}$ according to the regions as $\tilde{c} = \tilde{c}^{(\mathrm{i})} \chi_{\tilde{D}} + \tilde{c}^{(\mathrm{o})} \chi_{\mathbb{R}^2 \setminus \tilde{D}}$, i.e., let $\tilde{c}^{(\mathrm{i})}$ denotes the nutrient solution inside the tumor, and $\tilde{c}^{(\mathrm{o})}$ presents the outside solution. Then, the continuity at the boundary yields

$$(3.19\mathrm{a}) \qquad \tilde{c}^{(\mathrm{i})}(Z + \delta \mathcal{P}_l(\vartheta), \vartheta, t) = \tilde{c}^{(\mathrm{o})}(Z + \delta \mathcal{P}_l(\vartheta), \vartheta, t), \qquad \forall \vartheta \in \mathcal{R}$$

$$(3.19\mathrm{b}) \qquad \partial_\zeta \tilde{c}^{(\mathrm{i})}(Z + \delta \mathcal{P}_l(\vartheta), \vartheta, t) = \partial_\zeta \tilde{c}^{(\mathrm{o})}(Z + \delta \mathcal{P}_l(\vartheta), \vartheta, t), \qquad \forall \vartheta \in \mathcal{R},$$

With the same spirit of (3.17), for $\partial_\zeta \tilde{c}(Z + \delta \mathcal{P}_l(\vartheta), \vartheta, t)$ we have
$$(3.20)$$
$$\partial_\zeta \tilde{c}(Z + \delta \mathcal{P}_l(\vartheta), \vartheta, t) = \partial_\zeta c_0(Z, t) + \partial_\zeta^2 c_0(Z, t) \delta \mathcal{P}_l(\vartheta) + \partial_\zeta c_1(Z, t) \delta \mathcal{P}_l(\vartheta) + O(\delta^2).$$

Since c_0 is the solution to the unperturbed problem (given by (2.32) or (2.23) for the respect case), c_0 and c_0' are both continuous at the unperturbed boundary $\mathcal{B}_t = \{\zeta = Z(t)\}$. More precisely,

$$(3.21) \qquad c_0^{(\mathrm{i})}(Z, t) = c_0^{(\mathrm{o})}(Z, t),$$

$$(3.22) \qquad \partial_\zeta c_0^{(\mathrm{i})}(Z, t) = \partial_\zeta c_0^{(\mathrm{o})}(Z, t).$$

Thus, by using the expansions (3.17) and (3.20), the boundary condition (3.19) yields

$$(3.23\mathrm{a}) \qquad c_1^{(\mathrm{i})}(Z, t) = c_1^{(\mathrm{o})}(Z, t),$$

$$(3.23\mathrm{b}) \qquad \partial_\zeta^2 c_0^{(\mathrm{i})}(Z, t) + \partial_\zeta c_1^{(\mathrm{i})}(Z, t) = \partial_\zeta^2 c_0^{(\mathrm{o})}(Z, t) + \partial_\zeta c_1^{(\mathrm{o})}(Z, t).$$

By using (3.18) or (3.23) as the boundary condition for c_1, we can work out the particular solution of c_1 in the respective cases. We mention that when the boundary is the traveling front, to carry out the full expression of c_1, we also need to use the boundary condition $c_1(-\infty, y) = c_1(+\infty, y) = 0$ for any $y \in \mathbb{R}$, which is derived from $\tilde{c}(-\infty, y) = 0$ and $\tilde{c}(+\infty, y) = c_B$ for any $y \in \mathbb{R}$. The detail calculations will be carried out for each specific case later (Section 4.2 and Section 5.2).

In either nutrient model, the perturbed pressure solution $\tilde{p}$ satisfies the boundary condition

$$(3.24) \qquad \tilde{p} = 0, \quad \text{at} \quad \tilde{\mathcal{B}}_t.$$

Similar to the previous calculations. By using the expansion (3.14b) to evaluate $\tilde{p}$ at $(Z + \delta \mathcal{P}_l(\vartheta)) \in \tilde{\mathcal{B}}_t$, we get

$$(3.25) \quad \tilde{p}(Z + \delta \mathcal{P}_l(\vartheta), \vartheta, t) = p_0(Z, t) + \partial_\zeta p_0(Z, t) \delta \mathcal{P}_l(\vartheta) + p_1(Z, t) \delta \mathcal{P}_l(\vartheta) + O(\delta^2).$$

The perturbed and unperturbed boundary condition yield that $\tilde{p}(Z + \delta \mathcal{P}_l(\vartheta), \vartheta, t)$ and $p_0(Z, t)$ both equal to zero. In particular, p_0 as the unperturbed solution has already been solved in the Section 2.2. Thus we get

$$(3.26) \qquad \partial_\zeta p_0(Z, t) + p_1(Z, t) = 0.$$

Then by using the expression of c_1 (see (3.15b)) and (3.26), we can further determine the particular solution of p_1. For the traveling wave case, we also use the condition $\partial_\zeta p_1(-\infty, y) = 0$ for $\forall y \in \mathbb{R}$. Finally, the normal boundary speed (2.10) yields:

$$(3.27) \qquad \frac{d(Z(t) + \delta(t) \mathcal{P}_l(\vartheta))}{dt} = -\partial_\zeta \tilde{p}(Z + \delta \mathcal{P}_l(\vartheta), \vartheta, t).$$

By plugging the expression of $\tilde{p}$ into (3.27) and taking Taylor expansion for the ζ variable, we get

(3.28)
$$\frac{dZ}{dt} + \frac{d\delta}{dt}\mathcal{P}_l(\vartheta) = -\left(\partial_\zeta p_0(Z,t) + \partial_\zeta^2 p_0(Z,t)\delta\mathcal{P}_l(\vartheta) + \partial_\zeta p_1(Z,t)\delta\mathcal{P}_l(\vartheta) + O(\delta^2)\right).$$

Since the unperturbed problem yields $\frac{dZ}{dt} = -\partial_\zeta p_0(Z,t)$, the above identity can be further simplified into

(3.29)
$$\delta^{-1}\frac{d\delta}{dt} = -\left(\partial_\zeta^2 p_0(Z,t) + \partial_\zeta p_1(Z,t) + O(\delta)\right).$$

In the end, we determine the evolution of the perturbation magnitude by the sign of $\delta^{-1}\frac{d\delta}{dt}$. If it is positive, then it implies the growing of the magnitude. For the radial case, $Z(t)$ is given by the unperturbed tumor radius $R(t)$, therefore $\delta^{-1}\frac{d\delta}{dt} \sim -(\partial_r^2 p_0(R(t),t) + \partial_r p_1(R(t),t))$. Note that the leading order of $\delta^{-1}\frac{d\delta}{dt}$ is independent on θ, which parameterize the boundaries. While, for the traveling wave case, $Z(t) = 0$, thus $\delta^{-1}\frac{d\delta}{dt} \sim -(\partial_\xi^2 p_0(0) + \partial_\xi p_1(0))$, which is independent of y. Furthermore, under the same nutrient regime, we expect that the boundary instability of the radius case will coincide with that of the traveling wave when R increase to infinity.

4. Stability of traveling waves in the two nutrient models

In this section, we study the boundary stability of the traveling wave front under two nutrient regimes. In Section 4.1, we establish the set up and main conclusions. In Section 4.2, we work out the expression of $\delta^{-1}\frac{d\delta}{dt}$ for the two nutrient models, which serves as the proof of Theorem 4.1. And in Section 4.3, we prove the mathematical properties of $\delta^{-1}\frac{d\delta}{dt}$ summarized in Corollary 4.2, and these properties further yield the boundary behaviors summarized in Remark 4.3.

4.1. **Setup and main results.** As presented in Section 3.1, in the traveling wave case we employ the Euler coordinate system (ξ, y). In the absence of perturbation, the tumor boundary is defined by (3.3) with the level set index $Z(t) = 0$, and the tumor region is the left half space $D(t) = \{(\xi, y)|\xi \leqslant 0\}$. Then following the framework of Section 3, we consider the perturbation by a single wave mode:

(4.1)
$$\mathcal{P}_l(y) = \cos ly \qquad \text{with} \quad l \in \mathbb{R}^+,$$

thus the perturbed boundary (3.5) writes:

(4.2)
$$\tilde{\mathcal{B}}_t(y) = \{(\xi, y)|\xi = \delta(t)\cos ly, y \in \mathbb{R}\},$$

and the perturbed tumor region becomes

(4.3)
$$\tilde{D}(t) = \{(\xi, y)|\xi \leqslant \delta(t)\cos ly, y \in \mathbb{R}\}.$$

Then correspond to the above perturbation, the perturbed solutions c and p solves (3.9). Note that we dropped the tilde of the perturbed solutions for simplicity. Further more, the perturbed solutions possess the asymptotic expansions:

(4.4a)
$$c(\xi, y, t) = c_0(\xi) + \delta(t)c_1(\xi, y) + O(\delta^2),$$

(4.4b)
$$p(\xi, y, t) = p_0(\xi) + \delta(t)p_1(\xi, y) + O(\delta^2),$$

where the leading order terms c_0 and p_0 correspond to the solution of the unperturbed problems, which have been solved in Section 2.2.1 and Section 2.2.2 for the respective

nutrient model. And the first order terms $c_1(\xi, y, t)$ and $p_1(\xi, y, t)$ can be further expanded as

$$(4.4c) \qquad c_1(\xi, y) = \Sigma_{k=1}^{\infty} c_1^k(\xi) \cos kly,$$

$$(4.4d) \qquad p_1(\xi, y) = \Sigma_{k=1}^{\infty} p_1^k(\xi) \cos kly.$$

with $l \in \mathbb{R}^+$, so that c_1 has the same periodicity as the boundary geometry. However, from the calculation later we will see that $c_1^k(\xi) = p_1^k(\xi) = 0$ for any $k \neq 1$.

For the *in vivo* model, we use the superscript (i) or (o) to denote the solution inside or outside the tumor region $\tilde{D}(t)$. Then according to (3.15a) and (3.15c) we have

$$(4.5a) \qquad -\Delta c_1^{(i)}(\xi, y) + \lambda c_1^{(i)}(\xi, y) = 0,$$

$$(4.5b) \qquad -\Delta c_1^{(o)}(\xi, y) + c_1^{(o)}(\xi, y) = 0.$$

And by using the expansion in (3.17) and (3.20), the series form of $c_1(\xi, y)$ in (4.4c), the boundary condition (3.19) yields

$$(4.6a) \qquad c_1^{(i),k}(0) = c_1^{(o),k}(0), \quad \forall k \in \mathbb{N}^+,$$

$$(4.6b) \qquad \partial_\xi c_1^{(i),k}(0) = \partial_\xi c_1^{(o),k}(0), \quad \forall k \geqslant 2,$$

$$(4.6c) \qquad \partial_\xi^2 c_0^{(i)}(0) + \partial_\xi c_1^{(i),1}(0) = \partial_\xi^2 c_0^{(o)}(0) + \partial_\xi c_1^{(o),1}(0).$$

Further more, the assumptions $c(-\infty, y) = 0$ and $c(+\infty, y) = c_B$ for any $y \in \mathbb{R}$ yields

$$(4.6d) \qquad c_1^{(i),k}(-\infty) = 0,$$

$$(4.6e) \qquad c_1^{(o),k}(+\infty) = 0,$$

for any $k \in \mathbb{N}^+$.

For the *in vitro* model, c presents the nutrient solution inside the tumor and equation (3.15a) writes

$$(4.7) \qquad -\Delta c_1(\xi, y) + \lambda c_1(\xi, y) = 0, \quad \text{in} \quad \tilde{D}(t).$$

By using (3.17) and the series expansion of c_1 in (4.4c), the boundary condition (3.16) yields:

$$(4.8a) \qquad \partial_\zeta c_0(0) + c_1^1(0) = 0.$$

$$(4.8b) \qquad c_1^k(0) = 0, \quad \forall k \geqslant 2.$$

and similar to the *in vivo* model, the assumption $c(-\infty, y) = 0$ for any $y \in \mathbb{R}$ gives

$$(4.8c) \qquad c_1^k(-\infty) = 0, \qquad \forall k \in \mathbb{N}^+.$$

Once $c_1(\xi, y)$ is determined, we can move on to the study of the first order term of pressure, i.e., $p_1(\xi, y)$. Under either nutrient regime, $p_1(\xi, y)$ satisfies the equation:

$$(4.9) \qquad -\Delta p_1(\xi, y) = G_0 c_1(\xi, y), \quad \text{in} \quad \tilde{D}(t).$$

By using the expansion (3.25), the series form of p_1 in (4.4d), the boundary condition (3.24) yields

$$(4.10a) \qquad \partial_\zeta p_0(0) + p_1^1(0) = 0,$$

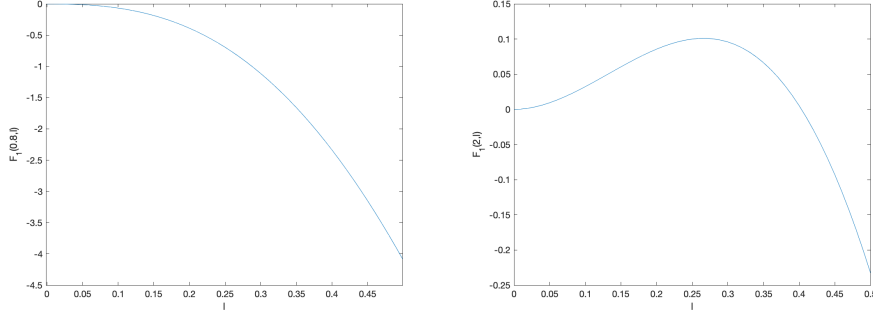$$(4.10b) \qquad p_1^k(0) = 0, \quad \forall k \geqslant 2.$$

FIGURE 1. $F_2(\lambda, l)$ for $G_0 = 1$, $c_B = 100$, left one: $\lambda = 0.8$, right one: $\lambda = 2$.

On the other hand, for the traveling wave case we require $\partial_\zeta p(-\infty, y) = 0$, which further yields $\partial_\xi p_1(-\infty, y) = 0$. Therefore,

$$(4.10c) \qquad \partial_\xi p_1^k(-\infty) = 0, \qquad \text{for} \quad \forall k \in \mathbb{N}^+.$$

Once the expression of $p_1(\xi, y)$ is determined, we can further work out the expression of $\delta^{-1}\frac{d\delta}{dt}$ for the two nutrient regimes, which determines the evolution of the perturbation amplitude. Now we establish the main conclusions, and the details of the calculation will be left to the next subsection.

Theorem 4.1. *Given growing rate $G_0 > 0$, background concentration $c_B > 0$, nutrient consumption rate $\lambda > 0$, and perturbation frequency $l \in \mathbb{R}^+$. The perturbation evolution function, $\delta^{-1}\frac{d\delta}{dt}$, of the* in vitro *model is given by:*

$$(4.11) \qquad \delta^{-1}\frac{d\delta}{dt} = \frac{G_0 c_B}{\sqrt{\lambda}} \cdot (\sqrt{\lambda} - \sqrt{\lambda + l^2}) + O(\delta) \stackrel{\text{def}}{=} F_1(\lambda, l) + O(\delta).$$

For the in vivo *model, $\delta^{-1}\frac{d\delta}{dt}$ is given by:*

$$(4.12) \qquad \delta^{-1}\frac{d\delta}{dt} = \frac{G_0 c_B}{\sqrt{\lambda}} \left(\frac{\sqrt{\lambda} - l}{\sqrt{\lambda} + 1} + \frac{l - \sqrt{\lambda + l^2}}{\sqrt{\lambda + l^2} + \sqrt{1 + l^2}} \right) + O(\delta)$$
$$\stackrel{\text{def}}{=} F_2(\lambda, l) + O(\delta).$$

Note that in either nutrient regime, the value of $G_0, c_B > 0$ serve as scaling parameters, therefore do not influence the quantitative behavior of $\delta^{-1}\frac{d\delta}{dt}$. For the *in vitro* model, one can easily check that $F_1(\lambda, l)$ is always negative. For the *in vivo* model, $F_2(\lambda, l)$ is plotted in Figure 1 for different choice of λ. Base on the expression of F_1, F_2, and the observations from Figure 1, we prove following mathematical properties for the evolution equations.

Corollary 4.2. *Fix $G_0 > 0$ and $c_B > 0$. For any $\lambda > 0$ and $l > 0$, $F_1(\lambda, l)$ in (4.11) is always negative, therefore the perturbation amplitude always decreases in the* in vitro *model. For the* in vivo *model, $\delta^{-1}\frac{d\delta}{dt}$ is given by $F_2(\lambda, l)$ as in (4.12). When l approaches zero, F_2 has the asymptote:*

$$(4.13a) \qquad F_2(\lambda, l) \sim \frac{(\lambda - 1) \cdot l^2 + O(l^3)}{2\lambda(\sqrt{\lambda + 1})(\sqrt{\lambda + l^2} + \sqrt{1 + l^2})},$$

and the limit at infinity:

$$(4.13b) \qquad \lim_{l \to +\infty} F_2(\lambda, l) \to -\infty.$$

Further more, for $\lambda > 1$ there exists $L > 0$ such that $F_2(\lambda, l) > 0$ for $l \in (0, L)$. And for $0 < \lambda \leqslant 1$, we have $F_2(\lambda, l) < 0$ for any $l > 0$. And in particular, when $\lambda = 1$, F_2 can be further simplified into:

$$(4.14) \qquad F_2(1, l) = \frac{l(1 - \sqrt{1 + l^2})}{2\sqrt{1 + l^2}} < 0, \qquad for \quad l > 0.$$

Remark 4.3. The mathematical properties of $F_2(\lambda, l)$ in Corollary 4.2 imply the following boundary behaviors:

(1) When the consumption rate is relatively large, the amplitude of low-frequency perturbations can grow in time, and the boundary propagation, therefore, becomes unstable. However, the amplitude of high-frequency perturbation decays. Correspondingly, the perturbed, wave like, boundary degenerates to the vertical line.

(2) When the nutrient consumption rate is relatively small, the perturbation amplitude decreases for perturbation of any frequency, i.e., the wave like boundary always evolve to a vertical line in this regime.

Remark 4.4. For either nutrient model, $\delta^{-1} \frac{d\delta}{dt} \to 0$ as $l \to 0$, we claim that this relate to the single wave perturbation of the radially symmetric solution as its radius R goes to infinity. This relationship will be further discussed in Section 5.4.

4.2. **The detailed calculations for the two nutrient regimes.** In this subsection we work out the expression of $\delta^{-1} \frac{d\delta}{dt}$ in Theorem 4.1 for the two nutrient models.

For the *in vivo* case. Plugging the expansion (4.4c) of $c_1(\xi, y)$ into (4.5), together with the conditions (4.6d) and (4.6e), for any $k \in \mathbb{N}^+$ we have:

$$(4.15a) \qquad c_1^{(i),k}(\xi) = a_1^k e^{\sqrt{\lambda + k^2}\xi} \qquad \text{for} \quad \xi \leqslant 0,$$

$$(4.15b) \qquad c_1^{(o),k}(\xi) = b_1^k e^{-\sqrt{1 + k^2}\xi} \qquad \text{for} \quad \xi \geqslant 0.$$

Recall that the leading order terms $c_0^{(i)}(\xi)$ and $c_0^{(o)}(\xi)$ are given by (2.23). Then (4.6a)-(4.6c) yield $a_1^k = b_1^k = 0$ for any $k \neq 1$, for $k = 1$ we get nontrivial solution:

$$(4.16) \qquad c_1^{(i),1}(\xi) = c_1^{(o),1}(\xi) = -\frac{\sqrt{\lambda} c_B}{\sqrt{\lambda + l^2} + \sqrt{1 + l^2}} e^{\sqrt{\lambda + l^2}\xi}.$$

By now, $c_1^{(i),k}(\xi)$ and $c_1^{(o),k}(\xi)$ are determined for any k. Therefore, $c_1(\xi, y)$ is determined. Then by solving equation (4.9) together with boundary conditions (4.10) (with p_0 given by (2.24)), we get $p_1^k(\xi) = 0$ for any $k \neq 1$, and:

$$(4.17a) \quad p_1^1(\xi) = A e^{l\xi} - \frac{G_0}{\lambda} c_1^{(i),1}(\xi) = A e^{l\xi} + \frac{G_0 c_B}{\sqrt{\lambda}(\sqrt{\lambda + l^2} + \sqrt{1 + l^2})} e^{\sqrt{\lambda + l^2}\xi},$$

with A given by:

$$(4.17b) \qquad A = \frac{G_0 c_B}{\sqrt{\lambda}} \left(\frac{1}{\sqrt{\lambda} + 1} - \frac{1}{\sqrt{\lambda + l^2} + \sqrt{1 + l^2}} \right).$$

By using the expression of $p_0(\xi)$ and $p_1^1(\xi)$, (3.29) yields that up to an error of $O(\delta)$:

$$(4.18) \qquad \delta^{-1}\frac{d\delta}{dt} = -\left(\partial_\xi^2 p_0(0) + \partial_\xi p_1^1(0)\right)$$

$$= \frac{G_0 c_B}{\sqrt{\lambda}}\left(\frac{\sqrt{\lambda}-l}{\sqrt{\lambda}+1} + \frac{l-\sqrt{\lambda+l^2}}{\sqrt{\lambda+l^2}+\sqrt{1+l^2}}\right) = F_2(\lambda, l).$$

For the *in vitro* model. Plugging the expansion of $c_1(\xi, y)$ (4.4c) into (4.7), together with the conditions (4.8c), for any $k \in \mathbb{N}^+$ we have:

$$(4.19) \qquad c_1^k(\xi) = a_1^k e^{\sqrt{\lambda+k^2}\xi} \qquad \text{for} \quad \xi \leqslant 0.$$

And the leading order term $c_0(\xi)$ for this case is given by (2.19). Then by using boundary condition (4.8), we get $c_1^k(\xi) = 0$ for any $k \neq 1$, and for $k = 1$:

$$(4.20) \qquad c_1^1(\xi) = -c_B\sqrt{\lambda}e^{\sqrt{\lambda+l^2}\xi}.$$

Then similar to the previous case, by solving equation (4.9) together with boundary conditions (4.10) (with p_0 given by (2.20)), we get $p_1^k(\xi) = 0$ for any $k \neq 1$. And for $k = 1$:

$$(4.21) \qquad p_1^1(\xi) = \frac{G_0 c_B}{\sqrt{\lambda}}e^{\sqrt{\lambda+l^2}\xi}.$$

Finally, by using the expression of p_0 and p_1^1, (3.29) yields up to an error of $O(\delta)$:

$$(4.22) \qquad \delta^{-1}\frac{d\delta}{dt} = -\left(\partial_\xi^2 p_0(0) + \partial_\xi p_1^1(0)\right)$$

$$= \frac{G_0 c_B}{\sqrt{\lambda}}(\sqrt{\lambda} - \sqrt{\lambda+l^2}) = F_1(\lambda, l).$$

By now we complete the proof of Theorem 4.1.

4.3. **Boundary stability analysis for the two nutrient models.** In this subsection, we prove the mathematical properties of F_1 and F_2 in Corollary 4.2, which further yields the boundary behaviors in Remark 4.3.

For the *in vitro* model, one can easily check that $F_1(\lambda, l) \leqslant 0$ for any frequency $l \geqslant 0$. Thus, the amplitude of the perturbation decays as time evolves for any single frequency perturbation. Therefore, the proof of the argument for the *in vitro* model in Corollary 4.2 is completed.

For the *in vivo* model, $\delta^{-1}\frac{d\delta}{dt}$ is given by (4.12) and plotted in Figure 1. The limit (4.13b) is obviously for checking. For the asymptote of l approaches 0, note that

$$(4.23) \qquad F_2(\lambda, l) = \frac{(\sqrt{\lambda}-l)(\sqrt{\lambda+l^2}+\sqrt{1+l^2})+(l-\sqrt{\lambda+l^2})(\sqrt{\lambda}+1)}{\sqrt{\lambda}(\sqrt{\lambda}+1)(\sqrt{\lambda+l^2}+\sqrt{1+l^2})}$$

$$= \frac{N(\lambda, l)}{2\lambda(\sqrt{\lambda}+1)(\sqrt{\lambda+l^2}+\sqrt{1+l^2})}.$$

By using the Taylor expansion $\sqrt{1+x} = 1 + \frac{x}{2} + O(x^2)$, when l approaches to 0 we have

$$(4.24) \qquad N(\lambda, l) = \frac{\lambda-1}{2\sqrt{\lambda}}l^2 + O(l^3).$$

Therefore, if $\lambda > 1$ then $F_2(\lambda, l) > 0$ for l close to zero, and $F_2(\lambda, l) < 0$ for l sufficiently large. Thus, by the intermediate value theorem and the continuity of $F_2(\lambda, l)$ in l, there exists $L > 0$ such that $F_2(\lambda, l) > 0$ for $l \in (0, L)$.

Now, we prove $F_2(\lambda, l) < 0$ for any $0 < \lambda \leqslant 1$ and $l > 0$. From the expression in (4.12), $F_2(\lambda, l) < 0$ hold obviously for $l \geqslant \sqrt{\lambda}$. On the other hand, the denominator in (4.23) is always positive. Therefore, it is sufficient for us to show the numerator $N(\lambda, l)$ is negative for $0 < l < \sqrt{\lambda} \leqslant 1$. Indeed, by taking the derivative of $N(\lambda, l)$ with respect to l, we get

$$(4.25) \quad \frac{\partial N(\lambda, l)}{\partial l} = -(\sqrt{\lambda + l^2} + \sqrt{1 + l^2}) + (\sqrt{\lambda} + 1) + \frac{-l(l+1)}{\sqrt{\lambda + l^2}} + \frac{l(\sqrt{\lambda} - l)}{\sqrt{1 + l^2}}$$

$$\leqslant -\frac{l(l+1)}{\sqrt{\lambda + l^2}} + \frac{l(\sqrt{\lambda} - l)}{\sqrt{1 + l^2}}$$

$$\leqslant \frac{l(\sqrt{\lambda} - 1 - 2l)}{\sqrt{\lambda + l^2}} < 0.$$

for $0 < l < \sqrt{\lambda} \leqslant 1$. Finally, combine with the fact $N(\lambda, 0) = 0$, we can conclude $N(\lambda, l) < 0$ for $0 < l < \sqrt{\lambda} \leqslant 1$. By now, we complete the proof of Corollary 4.2.

5. Stability of radially symmetric boundary in the two nutrient models

In this section, we study the boundary stability of the radially symmetric solution under the two nutrient regimes. The structure of this section is arranged as follow. We establish the setups and main conclusions in Section 5.1. After that we carry out the calculation of $\delta^{-1}\frac{d\delta}{dt}$ for the two nutrient models in Section 5.2, which serves as the proof of Theorem 5.1. Then, we proof the mathematical properties of the perturbation evolution functions summarized in Corollary 5.5 in Section 5.3. Finally, we discuss the relationship between the perturbation of the radial boundary and the traveling wave boundary in Section 5.4.

5.1. **Setup and main results.** For the radial case, we employ the polar coordinate system (r, θ). Before the perturbation, the tumor boundary is defined by (3.3) with the level set index $Z(t) = R(t)$, and the tumor region corresponds to the disk with radius $R(t)$, $D(t) = \{(r, \theta)|r \leqslant R(t)\}$. Following the framework of Section 3, we consider the perturbation by a single wave mode, i.e. $\mathcal{P}_l(\theta) = \cos l\theta$ with $\theta \in [-\pi, \pi)$. Then, the perturbed boundary (3.5) writes:

$$(5.1) \qquad \tilde{\mathcal{B}}_t(\theta) = \{(r, \theta)|r = R(t) + \delta(t)\cos l\theta, \theta \in [-\pi, \pi)\}.$$

Then the perturbed solutions (drop the tilde) c and p solves (3.9), with the perturbed tumor region $\tilde{D}(t)$ enclosed by $\tilde{\mathcal{B}}_t(\theta)$. Further more, c and p have the asymptotic expansions:

$$(5.2a) \qquad c(r, \theta, t) = c_0(r, t) + \delta(t)c_1(r, \theta, t) + O(\delta^2),$$

$$(5.2b) \qquad p(r, \theta, t) = p_0(r, t) + \delta(t)p_1(r, \theta, t) + O(\delta^2),$$

where the leading order terms c_0 and p_0 correspond to the unperturbed solutions for the respective nutrient model solved in Section 2.2.3 and Section 2.2.4. And the first order terms $c_1(r, \theta, t)$ and $p_1(r, \theta, t)$ can be further expanded as

$$(5.2c) \qquad c_1(r, \theta, t) = \Sigma_{k=1}^{\infty} c_1^k(r, t)\cos kl\theta,$$

(5.2d)
$$p_1(r, \theta, t) = \Sigma_{k=1}^{\infty} p_1^k(r, t) \cos kl\theta.$$

where l as the perturbation wave number is a positive integer. And from the calculation we will verify that $c_1^k(r, t) = p_1^k(r, t) = 0$ for any $k \neq 1$.

For the *in vivo* model, same as before we use the superscript (i) or (o) to denote the solution inside or outside the tumor region $\tilde{D}(t)$. Then according to (3.15a) and (3.15c) we have

(5.3a)
$$-\Delta c_1^{(i)}(r, \theta, t) + \lambda c_1^{(i)}(r, \theta, t) = 0,$$

(5.3b)
$$-\Delta c_1^{(o)}(r, \theta, t) + c_1^{(o)}(r, \theta, t) = 0.$$

and the Laplacian operator writes: $\Delta = \frac{\partial^2}{\partial r^2} + \frac{1}{r}\frac{\partial}{\partial r} + \frac{1}{r^2}\frac{\partial^2}{\partial \theta^2}$. By using the expansion in (3.17) and (3.20), the series form of $c_1(\xi, y)$ in (5.2c), the boundary condition (3.19) yields

(5.4a)
$$c_1^{(i),k}(R(t), t) = c_1^{(o),k}(R(t), t), \quad \forall k \in \mathbb{N}^+,$$

(5.4b)
$$\partial_r c_1^{(i),k}(R(t), t) = \partial_r c_1^{(o),k}(R(t), t), \quad \forall k \geq 2,$$

(5.4c)
$$\partial_r^2 c_0^{(i)}(R(t), t) + \partial_r c_1^{(i),1}(R(t), t) = \partial_r^2 c_0^{(o)}(R(t), t) + \partial_r c_1^{(o),1}(R(t), t).$$

In addition, the assumptions $c(0, \theta) < +\infty$ and $c(+\infty, \theta) = c_B$ for any $\theta \in [-\pi, \pi)$ yield that

(5.4d)
$$c_1^{(i),k}(0, t) < +\infty,$$

(5.4e)
$$c_1^{(o),k}(+\infty, t) = 0,$$

for any $k \in \mathbb{N}^+$.

For the *in vitro* model, c presents the nutrient solution inside the tumor and equation (3.15a) writes

(5.5)
$$-\Delta c_1(r, \theta, t) + \lambda c_1(r, \theta, t) = 0, \quad \text{in} \quad \tilde{D}(t).$$

And by using (3.17) and the series expansion of c_1 in (5.2c), the boundary condition (3.16) yields:

(5.6a)
$$\partial_\zeta c_0(R(t), t) + c_1^1(R(t), t) = 0.$$

(5.6b)
$$c_1^k(R(t), t) = 0, \quad \forall k \geq 2.$$

Similar to the *in vivo* model, the boundary condition (5.4d) remains ture (drop the superscript (i)).

Once $c_1(r, \theta, t)$ is determined by the boundary value problems above, we can further determine $p_1(r, \theta, t)$ for the corresponding model. Under either nutrient regime, $p_1(r, \theta, t)$ satisfies the equation:

(5.7)
$$-\Delta p_1(r, \theta, t) = G_0 c_1(r, \theta, t), \quad \text{in} \quad \tilde{D}(t).$$

By using the expansion (3.25), the series form of p_1 in (5.2d), the boundary condition (3.24) yields

(5.8a)
$$\partial_r p_0(R(t), t) + p_1^1(R(t), t) = 0.$$

(5.8b)
$$p_1^k(R(t), t) = 0, \quad \forall k \geq 2.$$

And by asymmetry we also have $\partial_r p(0, \theta, t) = 0$, which further provides

(5.8c)
$$\partial_r p_1^k(0, t) = 0, \quad \text{for} \quad \forall k \in \mathbb{N}^+.$$

Once $p_1(r, \theta, t)$ are determined, we can work out the expression of $\delta^{-1}\frac{d\delta}{dt}$ for the two nutrient regimes as in (3.29), which further determines the evolution of the perturbation amplitude. Now we establish the main conclusions, and the detailed calculation will be left to the next subsection.

Theorem 5.1. *Given growing rate $G_0 > 0$, background concentration $c_B > 0$, nutrient consumption rate $\lambda > 0$, and perturbation wave number $l \in \mathbb{N}^+$. When the radius of the tumor is around R (the corresponding unperturbed tumor has radius R), the evolution function $\delta^{-1}\frac{d\delta}{dt}$ for the* in vitro *model is given by:*
(5.9)
$$\delta^{-1}\frac{d\delta}{dt} = \frac{G_0 c_B I_1(\sqrt{\lambda}R)}{I_0(\sqrt{\lambda}R)}\left(\frac{I_1'(\sqrt{\lambda}R)}{I_1(\sqrt{\lambda}R)} - \frac{I_l'(\sqrt{\lambda}R)}{I_l(\sqrt{\lambda}R)}\right) + O(\delta) \overset{\text{def}}{=} F_3(\lambda, l, R) + O(\delta).$$

For the in vivo *model, $\delta^{-1}\frac{d\delta}{dt}$ is given by:*
(5.10)
$$\delta^{-1}\frac{d\delta}{dt} = \frac{G_0 c_B l}{\sqrt{\lambda}RC(R)}\left(\frac{C_1(R)}{C_l(R)}K_l(R)I_l(\sqrt{\lambda}R) - K_1(R)I_1(\sqrt{\lambda}R)\right)$$
$$- \frac{G_0 c_B}{C(R)}\left(\frac{C_1(R)}{C_l(R)}K_l(R)I_l'(\sqrt{\lambda}R) - K_1(R)I_1'(\sqrt{\lambda}R)\right) + O(\delta)$$
$$\overset{\text{def}}{=} F_4(\lambda, l, R) + O(\delta)$$

where $C(R)$ is defined in (2.33), and $C_j(R)$ ($j \in \mathbb{N}^+$) is given by
(5.11)
$$C_j(R) = K_j'(R)I_j(\sqrt{\lambda}R) - \sqrt{\lambda}I_j'(\sqrt{\lambda}R)K_j(R).$$

Since the results are presented in terms of the Bessel functions, we review the basic properties of them in Appendix A. Also note that in either nutrient regime, the value of $G_0, c_B > 0$ serve as scaling parameters, therefore do not influence the quantitative behavior of $\delta^{-1}\frac{d\delta}{dt}$. For the *in vitro* model, we will show that $F_3(\lambda, l, R)$ is always negative. For the *in vivo* model, fix the value of $G_0, c_B > 0$, $F_4(\lambda, l, R)$ is plotted in Figure 2 for different choice of λ and perturbation wave number l. Base on the expression of $\delta^{-1}\frac{d\delta}{dt}$ for the two nutrient models and the Figure 2, we establish following remarks.

Remark 5.2. $F_3(\lambda, 1, R) = F_4(\lambda, 1, R) = 0$ for any $\lambda, R > 0$. Since the mode 1 perturbation corresponds to a trivial translation instead of the change of boundary geometry.

Remark 5.3. When $0 < \lambda \leqslant 1$, fix any wave number $l \geqslant 2$, $F_4(\lambda, l, R)$ is always negative and monotone increases in R. Physically, when the nutrient consumption rate is relatively low, the perturbation amplitude continuously decreases to zero, regardless of the perturbation wave number and tumor size. Correspondingly, the tumor always evolves from a star shape to a larger disk.

Remark 5.4. For the regime $\lambda > 1$, we have:
   (1) For any fixed $l \geqslant 2$, there exists a threshold $R^*(l)$ such that $F_4(\lambda, l, R) < 0$ for $0 < R < R^*(l)$, and $F_4(\lambda, l, R) > 0$ for $R > R^*(l)$ (see the left top picture in Figure 2). That means considering any single wave perturbation, and assume the nutrient consumption rate is significant, the perturbation amplitude will degenerate while the tumor size is relatively small, and the tumor will evolve from a star shape to a larger disk as in the *in vitro* case. However, when the tumor size becomes large enough, the amplitude of the
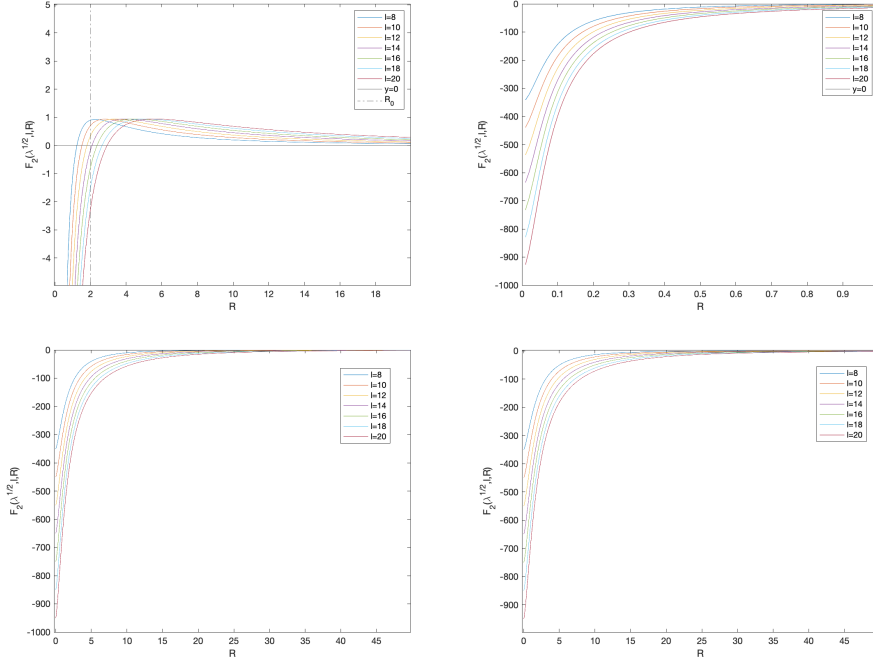
FIGURE 2. Graphs of F_4 with $G_0 = 1$, $c_B = 100$; top (left): $\lambda = 100$ and $R \in [0, 20]$; top (right): $\lambda = 100$ and $R \in [0, 1]$; bottom (left): $\lambda = 1$ and $R \in [0, 50]$; bottom (right): $\lambda = 0.8$ and $R \in [0, 50]$.

perturbation start to increase, and the tumor therefore remains in a star shape (but with a larger size).

(2) Fix a proper value of R_0, there exists l_0 such that $F_4(\lambda, l, R_0) > 0$ for $l < l_0$ and $F_4(\lambda, l, R_0) < 0$ for $l > l_0$ (see the left top picture in Figure 2), which implies that when the tumor size is around R_0 the perturbation of lower frequencies is easier to become unstable. See Figure 3 for the evolution of tumors under different perturbation wave numbers, where the blue curves correspond to the initial perturbed boundaries, and the red curves present the tumors evolve after a certain time.

(3) As the tumor size expands, $R(t)$ exceeds more thresholds $R^*(l)$, therefore the corresponding wave number perturbation become unstable successively.

Some of the results in the above remarks can be proved rigorously, we summarize them in the following Corollary and the proof is left to Section 5.3.

Corollary 5.5. *Fix $G_0 > 0$ and $c_B > 0$. For any $\lambda > 0$ and $l > 0$, $F_3(\lambda, l, R)$ is always negative, therefore the perturbation amplitude always decays for the* in vitro *model. For the* in vivo *model, we are able to show that for any $\lambda > 0$,*

$$(5.12a) \qquad F_4(\lambda, l, R) \sim G_0 c_B \frac{1-l}{2} \qquad\qquad as \quad R \sim 0,$$

$$(5.12b) \qquad F_4(\lambda, l, R) \sim G_0 c_B \frac{5(l^2 - 1)(\sqrt{\lambda} - 1)}{16\lambda R^2(\sqrt{\lambda} + 1)} \qquad as \quad R \sim +\infty.$$
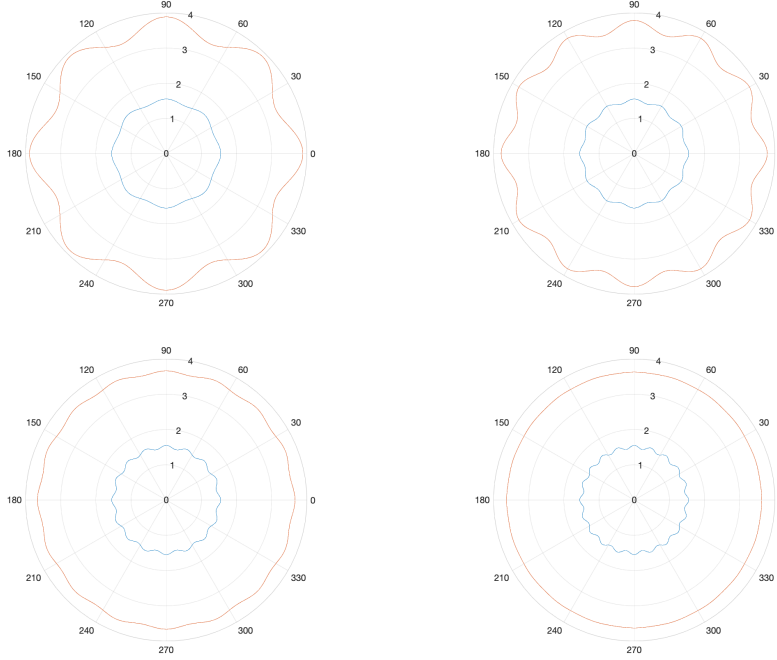
FIGURE 3. Evolution of tumor boundary for the *in vivo* model
with parameters: $G_0 = 1$, $c_B = 100$, $\lambda = 100$, $R_0 = 1.5$, $\delta = 0.05$,
$T = 2$. Wave numbers from left to right and top to bottom: $l = 8$,
$l = 12$, $l = 16$, $l = 20$.

Therefore, when $\lambda > 1$ and $l \geqslant 2$ there exists $R^*(l)$ such that $F_4(\lambda, l, R^*(l)) = 0$. In
addition, for $\lambda = 1$ and $l \geqslant 2$, $F_4(1, l, R)$ can be simplified into a simpler form:

$$(5.13) \quad \frac{1}{c_B G_0} F_4(1, l, R) = \sum_{j=1}^{l-1} R\Big(K_j(R)I_{j+1}(R) - K_{j+1}(R)I_{j+2}(R)\Big) - K_1(R)I_1(R).$$

Note that to fully prove the observations in Remark 5.3 and Remark 5.4, besides
the asymptotes given in Corollary 5.5, one also need to prove some monotonicity
results of $F_4(\lambda, l, R)$ with respect to the variable R or l. Unfortunately, we fail to
carry out the proof of that even for the special case $\lambda = 1$.

5.2. **The detailed calculations for the two nutrient regimes.** In this subsec-
tion we carry out the details of finding the expression of $\delta^{-1} \frac{d\delta}{dt}$ for the two nutrient
models, which completes the proof of theorem 5.1.

For the *in vivo* case. Plugging the expansion (5.2c) of $c_1(\xi, y)$ into (5.3), together
with the conditions (5.4d) and (5.4e), for any $k \in \mathbb{N}^+$ we have:

$$(5.14a) \qquad c_1^{(i),k}(r, t) = c_B a_1^k(t) I_{kl}(\sqrt{\lambda} r) \qquad \text{for} \quad r \leqslant R(t),$$

$$(5.14b) \qquad c_1^{(o),k}(r, t) = c_B b_1^k(t) K_{kl}(r) \qquad \text{for} \quad r \geqslant R(t).$$

Recall that the leading order terms $c_0^{(i)}(\xi)$ and $c_0^{(o)}(\xi)$ are given by (2.32). Then
(5.4a)-(5.4c) yield $a_1^k = b_1^k = 0$ for any $k \neq 1$, since I_j and K_j have the same sign,

but I'_j and K'_j have the opposite sign, while for $k = 1$, we get nontrivial solutions

$$(5.15a) \qquad a_1^1(t) = \frac{\left(a_0(R(t))\lambda I'_1(\sqrt{\lambda}R(t)) + b_0(R(t))K'_1(R(t))\right)K_l(R(t))}{C_l(R(t))},$$

$$(5.15b) \qquad b_1^1(t) = \frac{\left(a_0(R(t))\lambda I'_1(\sqrt{\lambda}R(t)) + b_0(R(t))K'_1(R(t))\right)I_l(\sqrt{\lambda}R(t))}{C_l(R(t))}.$$

where $C_l(R(t))$ is defined by (5.11), and $a_0(R(t))$ and $b_0(R(t))$ are given by (2.33). Note that $a_1^1(t)$ and $b_1^1(t)$ are depend on t via the tumor radius $R(t)$, therefore we write $a_1^1(R)$ instead of $a_1^1(t)$ in the following, and similarly for $b_1^1(R)$.

By now, $c_1^k(r,t)$ is determined for all k, therefore $c_1(r,\theta,t)$ is also determined. Then by solving equation (5.7) with expansion (5.2d) and the boundary conditions in (5.8) (with p_0 given by (2.34)), we get $p_1^k(r,t) = 0$ for any $k \neq 1$, and:

$$(5.16a) \qquad p_1^1(r,t) = G_0 c_B\left(B_l(R)r^l - \frac{1}{\lambda}a_1^1(R)I_l(\sqrt{\lambda}r)\right)$$

with $B_l(R)$ given by:

$$(5.16b) \qquad B_l(R) = \frac{1}{R^l}\left(\frac{a_1^1(R)I_l(\sqrt{\lambda}R)}{\lambda} + \frac{a_0(R)I_1(\sqrt{\lambda}R)}{\sqrt{\lambda}}\right).$$

By using the expression of $p_0(r,t)$ and $p_1^1(r,t)$, (3.29) yields that up to an error of $O(\delta)$:

$$(5.17) \quad \delta^{-1}\frac{d\delta}{dt} = -\left(\partial_r^2 p_0(R,t) + \partial_r p_1^1(R,t)\right)$$

$$= G_0 c_B\left(a_0(R)I'_1(\sqrt{\lambda}R) - B_l(R)lR^{l-1} + \frac{a_1^1(R)I'_l(\sqrt{\lambda}R)}{\sqrt{\lambda}}\right)$$

$$= G_0 c_B\frac{l}{\sqrt{\lambda}R\cdot C(R)}\left(\frac{C_1(R)}{C_l(R)}K_l(R)I_l(\sqrt{\lambda}R) - K_1(R)I_1(\sqrt{\lambda}R)\right)$$

$$- G_0 c_B\frac{1}{C(R)}\left(\frac{C_1(R)}{C_l(R)}K_l(R)I'_l(\sqrt{\lambda}R) - K_1(R)I'_1(\sqrt{\lambda}R)\right)$$

$$\stackrel{\text{def}}{=} F_4(\lambda, l, R).$$

For the *in vitro* model. Plugging the expansion of $c_1(r,\theta,t)$ (5.2c) into (5.5), together with the conditions (5.4d), for any $k \in \mathbb{N}^+$ we have:

$$(5.18) \qquad c_1^k(r,t) = c_B a_1^k(t)I_{kl}(\sqrt{\lambda}r) \qquad \text{for} \quad r \leqslant R(t).$$

And the leading order term $c_0(r,t)$ for this case is given by (2.28). Then by using boundary condition (5.6), we get $a_1^k(t) = 0$ for any $k \neq 1$, since I_j is always positive. While for $k = 1$:

$$(5.19) \qquad a_1^1(R(t)) = -\frac{c_B\sqrt{\lambda}I_1(\sqrt{\lambda}R)}{I_0(\sqrt{\lambda}R)I_l(\sqrt{\lambda}R)}.$$

Then similar to the previous case, by solving equation (5.7) together with boundary conditions (5.8) (with p_0 given by (2.29)), we get $p_1^k(r,t) = 0$ for any $k \neq 1$. And for $k = 1$:

$$(5.20) \qquad p_1^1(r,t) = \frac{G_0 c_B I_1(\sqrt{\lambda}R)}{\sqrt{\lambda}I_0(\sqrt{\lambda}R)I_l(\sqrt{\lambda}R)}I_l(\sqrt{\lambda}r).$$

Finally, by using the expression of p_0 and p_1^1, (3.29) yields up to an error of $O(\delta)$:

$$(5.21) \qquad \delta^{-1}\frac{d\delta}{dt} = -\left(\partial_r^2 p_0(R,t) + \partial_r p_1^1(R,t)\right)$$

$$= \frac{G_0 c_B I_1(\sqrt{\lambda}R)}{I_0(\sqrt{\lambda}R)}\left(\frac{I_1'(\sqrt{\lambda}R)}{I_1(\sqrt{\lambda}R)} - \frac{I_l'(\sqrt{\lambda}R)}{I_l(\sqrt{\lambda}R)}\right) = F_3(\lambda, l, R).$$

5.3. **Boundary stability analysis for the two nutrient models.** In this subsection, we prove the mathematical properties of F_3 and F_4 summarized in Corollary 5.5 by using the properties for Bessel functions in the Appendix A.

For the *in vitro* model, $\delta^{-1}\frac{d\delta}{dt}$ is given by (5.9), which is negative for any $l \in \mathbb{N}^+$ and $c_B, G_0, \lambda, R > 0$. Indeed, observe that (5.9) can be written as:

$$(5.22) \qquad \delta^{-1}\frac{d\delta}{dt} = G_0 c_B \frac{I_1(\sqrt{\lambda}R)}{\sqrt{\lambda}R I_0(\sqrt{\lambda}R)} H_l(\sqrt{\lambda}R),$$

where $H_l(r) \overset{\text{def}}{=} r\left(\frac{I_1'(r)}{I_1(r)} - \frac{I_l'(r)}{I_l(r)}\right)$. It was checked that $H_l'(r) > 0$ for any $r > 0$ and $l \in \mathbb{N}+$ (see equation (2.19) in [27]). On the other hand, by using the asymptote of $I_l(r)$ in (A.5), one can check that $\lim_{r\to\infty} H_l(r) = 0$. Thus, $H_l(r) < 0$ for any $r > 0$ and wave number l, which further yields $\delta^{-1}\frac{d\delta}{dt}$ is negative as well. Therefore, the amplitude of the perturbation decays as time evolves for any wave number. By now, the proof of the argument for the *in vitro* model in Corollary 5.5 is completed.

For the *in vivo* model, $\delta^{-1}\frac{d\delta}{dt}$ is given by (5.10). Now we check the properties of $F_4(\lambda, l, R)$ established in Corollary 5.5. Observe that according to (5.10), the evolution function can be decomposed as $F_4(\lambda, l, R) = G_0 c_B(T_1 - T_2)$, where $T_1(\lambda, l, R)$ and $T_2(\lambda, l, R)$ are given by:

$$(5.23a) \qquad T_1(\lambda, l, R) = \frac{l}{\sqrt{\lambda}RC(R)}\left(\frac{C_1(R)}{C_l(R)}K_l(R)I_l(\sqrt{\lambda}R) - K_1(R)I_1(\sqrt{\lambda}R)\right),$$

$$(5.23b) \qquad T_2(\lambda, l, R) = \frac{1}{C(R)}\left(\frac{C_1(R)}{C_l(R)}K_l(R)I_l'(\sqrt{\lambda}R) - K_1(R)I_1'(\sqrt{\lambda}R)\right).$$

By using the asymptotes in (A.4) one can check that for any wave number $l \geqslant 2$:

$$(5.24a) \qquad\qquad T_1 \sim \frac{1-l}{2}, \qquad \text{as} \quad R \sim 0,$$

$$(5.24b) \qquad\qquad T_2 \sim 0, \qquad \text{as} \quad R \sim 0.$$

Therefore, $F_4(\lambda, l, R) \sim G_0 c_B \frac{1-l}{2} < 0$ as R approaches to zero (this can be observed in Figure 2).

On the other hand, by using the asymptotes at infinity: (A.5) and (A.6), we can also check that

$$(5.24\text{ca}) \qquad\qquad T_1 \sim \frac{l(1-10l^2)}{32\lambda R^3(\sqrt{\lambda}+1)} = O(\frac{1}{R^3}), \qquad \text{as} \quad R \sim +\infty,$$

$$(5.24\text{cb}) \qquad\qquad T_2 \sim \frac{5(1-l^2)(\sqrt{\lambda}-1)}{16\lambda R^2(\sqrt{\lambda}+1)}, \qquad \text{as} \quad R \sim +\infty,$$

which further yields

$$(5.24\text{d}) \qquad\qquad F_4(\lambda, l, R) \sim \frac{5(l^2-1)(\sqrt{\lambda}-1)}{16\lambda R^2(\sqrt{\lambda}+1)} + O(\frac{1}{R^3}) \quad \text{as} \quad R \sim +\infty.$$

Therefore, for $\lambda > 1$ by intermediate value theorem the function $F_4(\sqrt{\lambda}, l, R_0)$ must intersect the horizontal axis.

Now, we investigate the special case $\lambda = 1$. Firstly, observe that by using the identity (A.3), $F_4(\lambda, l, R)$ can be further written into:

(5.4)
$$F_4 = \frac{1}{C(R)} \left(K_1(R) I_2(\sqrt{\lambda}R) - \frac{C_1(R)}{C_l(R)} K_l(R) I_{l+1}(\sqrt{\lambda}R) - \frac{l-1}{\sqrt{\lambda}R} K_1(R) I_1(\sqrt{\lambda}R) \right).$$

Also note that when $\lambda = 1$, by using the Wronskians cross product (A.7), we get:

(5.5a) $\quad C(R) = I_0(R) K_1(R) + I_1(R) K_0(R) = \dfrac{1}{R},$

(5.5b) $\quad C_l(R) = -\dfrac{1}{2} \left((K_{l+1}(R) + K_{l-1}(R)) I_l(R) + (I_{l+1}(R) + I_{l-1}(R)) K_l(R) \right)$

$$= -\frac{1}{R} \quad \text{for} \quad \forall l \in \mathbb{N}.$$

Therefore, when $\lambda = 1$ we can further simplify $F_4(\lambda, l, R)$ into:

(5.6)
$$\frac{1}{c_B G_0} F_4(\lambda, l, R) = R\Big(K_1(R) I_2(R) - K_l(R) I_{l+1}(R) \Big) - (l-1) K_1(R) I_1(R)$$

$$= \sum_{j=1}^{l-1} R\Big(K_j(R) I_{j+1}(R) - K_{j+1}(R) I_{j+2}(R) \Big) - K_1(R) I_1(R).$$

5.4. **Relationship between the Radial boundary and the traveling wave boundary.** In the last section we discuss the relationship between the two kinds of boundaries. In Section 2.2 we have already checked that without the perturbation, the propagation speed of the radial boundary converges to that of the traveling wave boundary as the radius tends to infinity.

Now, we explore the relationship for the perturbed boundaries. As before, we use (r, θ) to present the polar coordinates, and (ξ, y) for the Euler coordinates. Considering the perturbation of the radial boundary, let $\tilde{y} = \theta * R(t)$ and $\tilde{l} = l/R(t)$. Then the perturbation part can be rewritten as:

(5.7) $$\mathcal{P}_l(\theta) = \cos l\theta = \cos \tilde{l}\tilde{y} \overset{\text{def}}{=} \mathcal{P}_\omega(\tilde{y})$$

with $\tilde{y} \in (-\pi R, \pi R)$. Moreover, as $R \to +\infty$, $\tilde{l}$ tends to zero and $\tilde{y} \in \mathbb{R}$.

Also note that we can map the unperturbed radial boundary, $r = R$, to the unperturbed traveling wave boundary, $\xi = 0$, by the map:

(5.8) $$(R, \theta) \mapsto (0, \tan \theta/2), \qquad \theta \in (-\pi, \pi).$$

Thus, as $R \to +\infty$ any radial perturbation with finite wave number l (defined by (5.1)) will converge to the perturbation of the traveling wave boundary (defined by (4.2)) but with the zero frequency. Further more, for the same nutrient model the following relationships of the amplitude evolution equations hold:

(5.9a) $$\lim_{R \to +\infty} F_3(\lambda, l, R) = F_1(\lambda, 0) = 0,$$

(5.9b) $$\lim_{R \to +\infty} F_4(\lambda, l, R) = F_2(\lambda, 0) = 0.$$

for any $\lambda > 0$ and $l \in \mathbb{N}^+$.

6. **Conclusion**

In this paper, we study the tumor boundary instability induced by nutrient consumption and supply in two scenarios: 1) the front of the traveling wave; 2) the radially symmetric boundary. In each scenario, we investigate the boundary behaviors under two different nutrient supply regimes, *in vitro* and *in vivo*.

For the traveling wave scenario, our analysis shows the boundary is stable for any frequency perturbation $l \in \mathbb{R}^+$ and positive consumption rate λ when the nutrient supply is governed by the *in vitro* regime. In contrast, for *in vivo* regime, there exists a threshold value L such that the perturbation with a frequency smaller than L becomes unstable when the nutrient consumption rate λ is larger than one.

Then we consider the radially symmetric boundary scenario to explore further the influence of the finite size effect on boundary stability/instability. Our analysis shows that the *in vitro* regime still suppresses the increase of perturbation amplitude and stabilizes the boundary regardless of the consumption rate λ, perturbation wave number $l \in \mathbb{N}$, and tumor size R. For the *in vivo* regime, when $\lambda \leqslant 1$, the boundary behaves identically the same as the *in vitro* case. However, when $\lambda > 1$, the continuous growth of tumor radius enables perturbation wave number l to become unstable in turn (from low to high). Further more, as R is approaching infinity, the results in the radial case connect to the counterparts in the traveling wave case.

In the end, we conjecture that symmetric breaking traveling wave solutions may exist in the *in vivo* nutrient regime. From Figure 4.1, one can observe that for proper large l there exists $\lambda_0 > 1$ such that $F_2(\lambda_0, l) = 0$, i.e., the perturbation amplitude δ, up to some higher order error, neither growing nor decaying for such parameters. Thus, it is reasonable to expect that one may get the symmetric breaking traveling wave solutions by carefully modifying the linear solutions around the parameter (λ_0, l). We speculate that the technique in [27] might be helpful in solving this conjecture, which we save for future studies.

Appendix A. **Properties of Bessel functions**

Since the solutions of the radial case are presented in terms of the second kind modified Bessel functions $I_n(r)$ and $K_n(r)$ (for $n \in \mathbb{N}$), we review some basic properties of them in this section. Firstly, $I_n(r)$ and $K_n(r)$ solve the differential equation:

$$r^2 \frac{d^2 f}{dr^2} + r \frac{df}{dr} - (r^2 + n^2)f = 0, \tag{A.1}$$

and are strict positive for any $n \in \mathbb{N}$ and $r > 0$. For the derivatives, we have $I_0'(r) = I_1(r) > 0$ and $K_0'(r) = -K_1(r) < 0$, and for $n \geqslant 1$:

$$I_n'(r) = \frac{I_{n-1}(r) + I_{n+1}(r)}{2} > 0, \tag{A.2a}$$

$$K_n'(r) = -\frac{K_{n-1}(r) + K_{n+1}(r)}{2} < 0. \tag{A.2b}$$

Therefore, $I_j(r)$ are monotone increasing functions, and $K_j(r)$ are monotone decreasing functions. And the Bessel function $I_n(r)$ satisfies:

$$I_n'(r) - \frac{n}{r} I_n(r) = I_{n+1}(r), \tag{A.3}$$

for any $n \in \mathbb{N}^+$.

When $r \to 0$, $I_n(r)$ and $K_n(r)$ possess following asymptotes:

$$I_n(r) \sim \frac{1}{\Gamma(n+1)} \left(\frac{r}{2}\right)^n, \qquad \text{for} \quad n \in \mathbb{N}, \tag{A.4a}$$

$$K_n(r) \sim \frac{\Gamma(n)}{2} \left(\frac{r}{2}\right)^{-n}, \qquad \text{for} \quad n \in \mathbb{N}^+, \tag{A.4b}$$

$$K_0(r) \sim -\ln r. \tag{A.4c}$$

While as $r \to +\infty$, $I_n(r)$ and $K_n(r)$ have the asymptotes:

$$I_n(r) \sim \left(\frac{1}{2\pi r}\right)^{1/2} e^r \left(1 - \frac{4n^2 - 1}{8r} + \frac{(4n^2 - 1)(4n^2 - 9)}{128 n^2} + O\left(\frac{1}{r^3}\right)\right), \tag{A.5a}$$

$$K_n(r) \sim \left(\frac{\pi}{2r}\right)^{1/2} e^{-r} \left(1 + \frac{4n^2 - 1}{8r} + \frac{(4n^2 - 1)(4n^2 - 9)}{128 r^2} + O\left(\frac{1}{r^3}\right)\right). \tag{A.5b}$$

By using (A.2), we can also derive the asymptotes for $I'(r)$ and $K'(r)$ for $r \to +\infty$:

$$I_n'(r) \sim \left(\frac{1}{2\pi r}\right)^{1/2} e^r \left(1 - \frac{4n^2 + 3}{8r} + \frac{(4n^2 - 1)(4n^2 + 15)}{128 r^2} + O\left(\frac{1}{r^3}\right)\right), \tag{A.6a}$$

$$K_n'(r) \sim -\left(\frac{1}{2\pi r}\right)^{1/2} e^{-r} \left(1 + \frac{4n^2 + 3}{8r} + \frac{(4n^2 - 1)(4n^2 + 15)}{128 r^2} + O\left(\frac{1}{r^3}\right)\right). \tag{A.6b}$$

Further more, $I_n(r)$ and $K_n(r)$ satisfy the so-called Wronskians cross product:

$$I_n(r) K_{n+1}(r) + I_{n+1}(r) K_n(r) = \frac{1}{r} \quad \text{for} \quad \forall n \in \mathbb{N}. \tag{A.7}$$

References

[1] John A Adam and Nicola Bellomo. *A survey of models for tumor-immune system dynamics*. Springer Science & Business Media, 2012.

[2] Robyn P Araujo and DL Sean McElwain. A history of the study of solid tumour growth: the contribution of mathematical modelling. *Bulletin of mathematical biology*, 66(5):1039–1091, 2004.

[3] DG Aronson, O Gil, and JL Vázquez. Limit behaviour of focusing solutions to nonlinear diffusions. *Communications in partial differential equations*, 23(1-2):197–206, 1998.

[4] Eshel Ben-Jacob, Ofer Schochet, Adam Tenenbaum, Inon Cohen, Andras Czirok, and Tamas Vicsek. Generic modelling of cooperative growth patterns in bacterial colonies. *Nature*, 368(6466):46–49, 1994.

[5] H. M. Byrne and M.A.J. Chaplain. Growth of necrotic tumors in the presence and absence of inhibitors. *Mathematical biosciences*, 135(2):187–216, 1996.

[6] Helen Byrne and Dirk Drasdo. Individual-based and continuum models of growing cell populations: a comparison. *Journal of mathematical biology*, 58(4):657–687, 2009.

[7] HM Byrne, T Alarcon, MR Owen, SD Webb, and PK Maini. Modelling aspects of cancer dynamics: a review. *Philosophical Transactions of the Royal Society A: Mathematical, Physical and Engineering Sciences*, 364(1843):1563–1578, 2006.

[8] MAJ Chaplain. Avascular growth, angiogenesis and vascular growth in solid tumours: The mathematical modelling of the stages of tumour development. *Mathematical and computer modelling*, 23(6):47–87, 1996.

[9] C Chatelain, T Balois, Pasquale Ciarletta, and M Ben Amar. Emergence of microstructural patterns in skin cancer: a phase separation analysis in a binary mixture. *New Journal of Physics*, 13(11):115013, 2011.

[10] Vittorio Cristini, Eugene Koay, and Zhihui Wang. *An introduction to physical oncology: How mechanistic mathematical modeling can improve cancer therapy outcomes*. CRC Press, 2017.

[11] Vittorio Cristini and John Lowengrub. *Multiscale modeling of cancer: an integrated experimental and mathematical modeling approach*. Cambridge University Press, 2010.

[12] Vittorio Cristini, John Lowengrub, and Qing Nie. Nonlinear simulation of tumor growth. *Journal of mathematical biology*, 46(3):191–224, 2003.

[13] Noemi David, Tomasz Debiec, and Benoît Perthame. Convergence rate for the incompressible limit of nonlinear diffusion-advection equations. *arXiv preprint arXiv:2108.00787*, 2021.

[14] Noemi David and Benoît Perthame. Free boundary limit of a tumor growth model with nutrient. *Journal de Mathématiques Pures et Appliquées*, 155:62–82, 2021.

[15] Noemi David and Markus Schmidtchen. On the incompressible limit for a tumour growth model incorporating convective effects. *arXiv preprint arXiv:2103.02564*, 2021.

[16] Xu'an Dou, Jian-Guo Liu, and Zhennan Zhou. A tumor growth model with autophagy: The reaction-(cross-) diffusion system and its free boundary limit. *Discrete and Continuous Dynamical Systems-B*, 2022.

[17] Marco A Fontelos and Avner Friedman. Symmetry-breaking bifurcations of free boundary problems in three dimensions. *Asymptotic Analysis*, 35(3-4):187–206, 2003.

[18] SJ Franks and JR King. Interactions between a uniformly proliferating tumour and its surroundings: uniform material properties. *Mathematical medicine and biology*, 20(1):47–89, 2003.

[19] SJ Franks and JR King. Interactions between a uniformly proliferating tumour and its surroundings: Stability analysis for variable material properties. *International journal of engineering science*, 47(11-12):1182–1192, 2009.

[20] Avner Friedman. A free boundary problem for a coupled system of elliptic, hyperbolic, and stokes equations modeling tumor growth. *Interfaces and Free boundaries*, 8(2):247–261, 2006.

[21] Avner Friedman and Bei Hu. Asymptotic stability for a free boundary problem arising in a tumor model. *Journal of Differential Equations*, 227(2):598–639, 2006.

[22] Avner Friedman and Bei Hu. Bifurcation from stability to instability for a free boundary problem arising in a tumor model. *Archive for rational mechanics and analysis*, 180(2):293–330, 2006.

[23] Avner Friedman and Bei Hu. Bifurcation for a free boundary problem modeling tumor growth by stokes equation. *SIAM Journal on Mathematical Analysis*, 39(1):174–194, 2007.

[24] Avner Friedman and Bei Hu. Bifurcation from stability to instability for a free boundary problem modeling tumor growth by stokes equation. *Journal of mathematical analysis and applications*, 327(1):643–664, 2007.

[25] Avner Friedman and Bei Hu. Stability and instability of liapunov-schmidt and hopf bifurcation for a free boundary problem arising in a tumor model. *Transactions of the American Mathematical Society*, 360(10):5291–5342, 2008.

[26] Avner Friedman and Fernando Reitich. Analysis of a mathematical model for the growth of tumors. *Journal of mathematical biology*, 38(3):262–284, 1999.

[27] Avner Friedman and Fernando Reitich. Symmetry-breaking bifurcation of analytic solutions to free boundary problems: an application to a model of tumor growth. *Transactions of the American Mathematical Society*, 353(4):1587–1634, 2001.

[28] Avner Friedman and Fernando Reitich. Quasi-static motion of a capillary drop, ii: the three-dimensional case. *Journal of Differential Equations*, 186(2):509–557, 2002.

[29] Avner Friedman and Fernando Reitich. Quasistatic motion of a capillary drop i. the two-dimensional case. *Journal of Differential Equations*, 178(1):212–263, 2002.

[30] O Gil and Fernando Quirós. Convergence of the porous media equation to hele-shaw. *Nonlinear Analysis: Theory, Methods & Applications*, 44(8):1111–1131, 2001.

[31] HP Greenspan. Models for the growth of a solid tumor by diffusion. *Studies in Applied Mathematics*, 51(4):317–340, 1972.

[32] HP Greenspan. On the growth and stability of cell cultures and solid tumors. *Journal of theoretical biology*, 56(1):229–242, 1976.

[33] Nestor Guillen, Inwon Kim, and Antoine Mellet. A hele-shaw limit without monotonicity. *Archive for Rational Mechanics and Analysis*, 243(2):829–868, 2022.

[34] Qingyou He, Hai-Liang Li, and Benoît Perthame. Incompressible limits of patlak-keller-segel model and its stationary state. *arXiv preprint arXiv:2203.13709*, 2022.

[35] Noureddine Igbida. The mesa-limit of the porous-medium equation and the hele-shaw problem. *Differential and Integral Equations*, 15(2):129–146, 2002.

[36] Matt Jacobs, Inwon Kim, and Jiajun Tong. Tumor growth with nutrients: Regularity and stability. *arXiv preprint arXiv:2204.07572*, 2022.

[37] Nick Jagiella. *Parameterization of Lattice-Based Tumor Models from Data*. PhD thesis, Université Pierre et Marie Curie-Paris VI, 2012.

[38] Inwon Kim, Antoine Mellet, and Yijing Wu. Density-constrained chemotaxis and hele-shaw flow. *arXiv preprint arXiv:2204.11917*, 2022.

[39] Inwon Kim and Norbert Požár. Porous medium equation to hele-shaw flow with general initial density. *Transactions of the American Mathematical Society*, 370(2):873–909, 2018.

[40] Inwon Kim, Norbert Požár, and Brent Woodhouse. Singular limit of the porous medium equation with a drift. *Advances in Mathematics*, 349:682–732, 2019.

[41] Inwon C Kim. Uniqueness and existence results on the hele-shaw and the stefan problems. *Archive for Rational Mechanics & Analysis*, 168(4), 2003.

[42] Inwon C Kim and Antoine Mellet. Homogenization of a hele–shaw problem in periodic and random media. *Archive for rational mechanics and analysis*, 194(2):507–530, 2009.

[43] Inwon C Kim, Benoît Perthame, and Panagiotis E Souganidis. Free boundary problems for tumor growth: a viscosity solutions approach. *Nonlinear Analysis*, 138:207–228, 2016.

[44] JR King and SJ Franks. Mathematical modelling of nutrient-limited tissue growth. In *Free Boundary Problems*, pages 273–282. Springer, 2006.

[45] Jian-Guo Liu, Min Tang, Li Wang, and Zhennan Zhou. An accurate front capturing scheme for tumor growth models with a free boundary limit. *Journal of Computational Physics*, 364:73–94, 2018.

[46] Jian-Guo Liu, Min Tang, Li Wang, and Zhennan Zhou. Analysis and computation of some tumor growth models with nutrient: From cell density models to free boundary dynamics. *Discrete and continuous dynamical systems. Series B*, 24(7):3011–3035, 2019.

[47] Jian-Guo Liu, Min Tang, Li Wang, and Zhennan Zhou. Toward understanding the boundary propagation speeds in tumor growth models. *SIAM Journal on Applied Mathematics*, 81(3):1052–1076, 2021.

[48] John S Lowengrub, Hermann B Frieboes, Fang Jin, Yao-Li Chuang, Xiangrong Li, Paul Macklin, Steven M Wise, and Vittorio Cristini. Nonlinear modelling of cancer: bridging the gap between cells and tumours. *Nonlinearity*, 23(1):R1, 2009.

[49] Min-Jhe Lu, Wenrui Hao, Chun Liu, John Lowengrub, and Shuwang Li. Nonlinear simulation of vascular tumor growth with chemotaxis and the control of necrosis. *Journal of Computational Physics*, 459:111153, 2022.

[50] Min-Jhe Lu, Chun Liu, and Shuwang Li. Nonlinear simulation of an elastic tumor-host interface. *Computational and Mathematical Biophysics*, 7(1):25–47, 2019.

[51] Min-Jhe Lu, Chun Liu, John Lowengrub, and Shuwang Li. Complex far-field geometries determine the stability of solid tumor growth with chemotaxis. *Bulletin of mathematical biology*, 82(3):1–41, 2020.

[52] Paul Macklin and John Lowengrub. Nonlinear simulation of the effect of microenvironment on tumor growth. *Journal of theoretical biology*, 245(4):677–704, 2007.

[53] Bertrand Maury, Aude Roudneff-Chupin, and Filippo Santambrogio. Congestion-driven dendritic growth. *Discrete & Continuous Dynamical Systems*, 34(4):1575, 2014.

[54] Antoine Mellet, Benoît Perthame, and Fernando Quiros. A hele–shaw problem for tumor growth. *Journal of Functional Analysis*, 273(10):3061–3093, 2017.

[55] William W Mullins and Robert F Sekerka. Morphological stability of a particle growing by diffusion or heat flow. *Journal of applied physics*, 34(2):323–329, 1963.

[56] Benoît Perthame. Some mathematical models of tumor growth. *Université Pierre et Marie Curie-Paris*, 6, 2016.

[57] Benoît Perthame, Fernando Quirós, and Juan Luis Vázquez. The hele–shaw asymptotics for mechanical models of tumor growth. *Archive for Rational Mechanics and Analysis*, 212(1):93–127, 2014.

[58] Benoît Perthame, Min Tang, and Nicolas Vauchelet. Traveling wave solution of the hele–shaw model of tumor growth with nutrient. *Mathematical Models and Methods in Applied Sciences*, 24(13):2601–2626, 2014.

[59] Benoît Perthame and Nicolas Vauchelet. Incompressible limit of a mechanical model of tumour growth with viscosity. *Philosophical Transactions of the Royal Society A: Mathematical, Physical and Engineering Sciences*, 373(2050):20140283, 2015.

[60] Kara Pham, Hermann B Frieboes, Vittorio Cristini, and John Lowengrub. Predictions of tumour morphological stability and evaluation against experimental observations. *Journal of the Royal Society Interface*, 8(54):16–29, 2011.

[61] Kara Pham, Emma Turian, Kai Liu, Shuwang Li, and John Lowengrub. Nonlinear studies of tumor morphological stability using a two-fluid flow model. *Journal of mathematical biology*, 77(3):671–709, 2018.

[62] Tiina Roose, S Jonathan Chapman, and Philip K Maini. Mathematical models of avascular tumor growth. *SIAM review*, 49(2):179–208, 2007.

[63] Min Tang, Nicolas Vauchelet, Ibrahim Cheddadi, Irene Vignon-Clementel, Dirk Drasdo, and Benoît Perthame. Composite waves for a cell population system modeling tumor growth and invasion. In *Partial Differential Equations: Theory, Control and Approximation*, pages 401–429. Springer, 2014.

[64] Emma Turian, Kai Liu, John Lowengrub, and Shuwang Li. Morphological stability of an elastic tumor–host interface. *Journal of Computational and Applied Mathematics*, 362:410–422, 2019.

[65] X Zheng, SM Wise, and V Cristini. Nonlinear simulation of tumor necrosis, neo-vascularization and tissue invasion via an adaptive finite-element/level-set method. *Bulletin of mathematical biology*, 67(2):211–259, 2005.

Yu Feng, Beijing International Center for Mathematical Research, Peking University, No. 5 Yiheyuan Road Haidian District, Beijing, P.R.China 100871
Email address: fengyu@bicmr.pku.edu.cn

Min Tang: School of Mathematical Sciences, Institute of Natural Sciences, MOE-LSC, Shanghai Jiao Tong University, Shanghai, 200240, P. R. China
Email address: tangmin@sjtu.edu.cn

Xiaoqian Xu: Zu Chongzhi Center for Mathematics and Computational Sciences, Duke Kunshan University, China
Email address: xiaoqian.xu@dukekunshan.edu.cn

Zhennan Zhou, Beijing International Center for Mathematical Research, Peking University, No. 5 Yiheyuan Road Haidian District, Beijing, P.R.China 100871
Email address: zhennan@bicmr.pku.edu.cn